A cost-effective and ecological stochastic optimization for integration of distributed energy resources in energy networks considering vehicle-to-grid and combined heat and power technologies

DARAMOLA, Alex S., IKPEHAI, Augustine, AHMADI, Seyed Ehsan and MARZBAND, Mousa

Journal of Energy Storage 57 (2023) 106203

Contents lists available at ScienceDirect

Journal of Energy Storage

journal homepage: www.elsevier.com/locate/est

Research papers

A cost-effective and ecological stochastic optimization for integration of distributed energy resources in energy networks considering vehicle-to-grid and combined heat and power technologies

Alex S. Daramola [a], Seyed Ehsan Ahmadi [a], Mousa Marzband [a,b,*], Augustine Ikpehai [c]

[a] Northumbria University, Electrical Power and Control Systems Research Group, Ellison Place NE1 8ST, Newcastle upon Tyne, UK
[b] Center of Research Excellence in Renewable Energy and Power Systems, King Abdulaziz University, Jeddah, 21589, Saudi Arabia
[c] Department of Engineering and Mathematics, Sheffield Hallam University, Sheffield S1 1WB, UK

ARTICLE INFO

Keywords:
distributed generation
Microgrid
CO_2 emission
Vehicle-to-grid
Combined heat and power
Fuel cell

ABSTRACT

Electric vehicles (EVs) have the potential to decarbonize the transport sector and contribute to the attainment of the global Net-Zero goal. However, to achieve sustainable decarbonization, EVs' power for grid-to-vehicle (G2V) operations should be sourced from carbon-free or low carbon power generating sources. Whilst the adoption of renewable energy sources (RES) in EVs' G2V process has been extensively explored, combined heat and power (CHP) technologies are underexamined. Hence, this paper deploys harmonized natural gas and fuel cell CHP technologies alongside RES and battery energy storage systems (BESS) to facilitate EVs' G2V and vehicle-to-grid (V2G) operations. While the BESS supports V2G operations and stores excess power from the CHP and RES, the CHP's by-product heat could be employed in heating homes and industrial facilities. Furthermore, to maximize environmental and economic benefits, the CHP technologies are designed following the hybrid electric-thermal load strategy, such that the system autonomously switches between following the electric load strategy and following the thermal load strategy. The proposed optimization problem is tested using three different case studies (CSs) to minimize the microgrid's (MG) operating costs and carbon dioxide (CO_2) emissions in a stochastic framework considering the RES generations, the load consumption, and the behaviour patterns of charging/discharging periods of EVs as the uncertain parameters. The first CS tests the proposed algorithm using only CHP technologies. Secondly, the algorithm is examined using the CHP technologies and RES. Finally, the BESS is added to support and analyse the impacts of the V2G operations of EVs on the MG. Furthermore, the life cycle assessment is investigated to analyse the CO_2 emissions of distributed generations. The results show a 32.22%, 44.49%, and 47.20% operating cost reduction in the first, second, and third CSs. At the same time, the CO_2 emissions declined by 29.13%, 47.13% and 47.90% in the various corresponding CSs. These results demonstrate the economic and environmental benefits of applying CHP with RES in facilitating G2V and V2G operations towards achieving a decarbonized transport sector.

1. Introduction

1.1. Motivation

Environmental sustainability is growing into a household discussion due to recent large-scale climate disasters such as the Attica wildfires in Greece, flooding in Australia, extensive wildlife migration and the unfavourable prevailing weather conditions. Although it cannot be ascertained with certainty how much average global temperature will increase, the significant impacts of global warming have been seen, and failing to take actions to prevent the consequences of further warming may show floundering [1]. To this end, climate change discussions have been at the forefront of governmental panels and meetings. The 2021 United Nations Climate Change Conference, commonly termed COP26, was explicitly set up to bring different global players and world leaders to discuss and agree on ways to mitigate greenhouse gas (GHG) emissions and keep the average global temperature of 1.5 °C within reach. Therefore, expediting the removal of fossil fuel-fired power plants and facilitating the switch to electric vehicles (EV) are proposed as some of the ways to secure global Net-Zero by 2050 [2]. However, the large-scale deployment of EVs leads to extensive network reinforcements, unbalanced voltage, increased load demand, raised operating costs and high electrical strain on the existing power distribution network. This

* Corresponding author at: Northumbria University, Electrical Power and Control Systems Research Group, Ellison Place NE1 8ST, Newcastle upon Tyne, UK.
E-mail address: mousa.marzband@northumbria.ac.uk (M. Marzband).

https://doi.org/10.1016/j.est.2022.106203
Received 19 May 2022; Received in revised form 1 November 2022; Accepted 19 November 2022
Available online 1 December 2022

Nomenclature

Acronyms

EV	Electric Vehicle
CHP	Combined heat and power
BESS	Battery energy storage system
CO_2	Carbon dioxide
V2G	Vehicle-to-grid
G2V	Grid-to-vehicle
GHG	Greenhouse gases
RES	Renewable energy sources
MG	Microgrid
PV	Photovoltaic
WT	Wind turbine
DG	Distributed generation
SBA	Scenario-Based Analysis
SoC	State of charge
PGU	Power generation unit
FELD	Following electrical load demand
FTLD	Following thermal load demand

Indices

K_{PGU}	Constant index of the PGU
K_{FCU}	Constant index of the fuel cell unit
K_{CHP}	Constant index of the CHP
γ_{NG}	Emission conversion factor of the natural gas
γ_{GRID}	Emission conversion factor of the grid

Parameters

η_{HRU}	Efficiency of the heat recovery unit [%]
η_{PGU}	Efficiency of the PGU [%]
η_{FR}	Efficiency of the fuel reformer [%]
η_{FCU}	Efficiency of the fuel cell unit [%]
η_{BOILER}	Boiler's thermal efficiency [%]
η^{EV+}, η^{EV-}	Charging/Discharging Efficiency of the EV [%]
T_{Ch}^{Day}, T_{Dch}^{Day}	Charging/ Discharging period of EV [Hours]
$SOC^{EV,\ Dep}$	State of charge of EV battery in departure time [%]
λ^{CO_2}	Price of CO_2 emission [£/kg CO_2]
μ_s	Probability of scenario s [0-1]

Decision variables

H_{FR}	Hydrogen from the fuel reformer [kg]
N_{FR}	Natural gas consumed by the fuel reformer [MMBTU/hour]
E_{PGU}	Total electricity derived from the [MWh]
N_{PGU}	Natural gas consumed by the PGU [MMBTU/hour]
E_{FCU}	Electricity generated by the fuel cell unit [MWh]
H_{FCU}	Hydrogen consumption of the fuel cell unit [kg]
Q_{PGU}, Q_{FR}	Heat recovered from the PGU/ fuel reformer [MMBTU/hour]
Q_{HRU}	Recovered heat passing through the heat recovery unit [MMBTU/day]
E_{total}^{CHP}	Total electricity produced by the CHP [MWh]
E_{req}	Electricity required by the EVs and buildings [MWh]
$Q_{req}^{bulding}$	Heat required to meet the building's heat load [MMBTU/hour]
Q_{BOILER}	Heat supplied by auxiliary boiler [MMBTU/hour]
E_{GRID}	Additional electricity purchased from the grid [MWh]
N_{TOTAL}	Total natural gas consumed by the PGU and fuel reformer [MMBTU]
N_{BOILER}	Natural gas consumed by the boiler [MMBTU/hour]
$Cost_{CHP\text{-}FHL}$	Cost of operating the CHP [GBP]
$CD_{Emission}$	Total CO_2 emission in the system [kg CO_2/MWh]
SOC_t^{EV}, SOC_t^{BESS}	Sate of charge of EV/ BESS at time t [Hours]
$\underline{SOC}_t^{BESS}$, $\overline{SOC}^{BESS}$	Minimum/ Maximum state of charge of BESS [%]
$\underline{SOC}^{EV}$, $\overline{SOC}^{EV}$	Minimum/ Maximum state of charge of EV [%]
P_{Total}^{EV}	Total energy that can be stored in the EV [MWh]
P_t^{EV+}, P_t^{EV-}	Charging/ Discharging power of the EV at time t [MW]
P_t^{PV}, P_t^{WT}, P_t^{CHP}	Power produced by the PV/ WT/ CHP at time t [MW]
P_t^{BESS-}, P_t^{BESS+}	Power supplied/ required by/ to charge the BESS at time t [MW]
P_t^{grid-}, P_t^{grid+}	Power purchased/ sold from/ to the grid at time t [MW]
$\overline{P}^{BESS+}$, $\overline{P}_t^{BESS-}$	Maximum power required/ discharged to charge/ by the BESS [MW]

paper explores a decentralized approach to alleviate some of these challenges and lower carbon dioxide (CO_2) emissions by investigating the integration of co-generation plants such as combined heat and power (CHP) and renewable energy technologies into the distribution network to support expansive EV use.

Currently, internal combustion engine (ICE) vehicles make up around 10% of universal carbon dioxide emissions, and oil-derived fuels account for roughly 95% of the energy expended in the transportation sector [3,4]. Conversely, CHP technologies can lower CO_2 emissions by around 32% compared to the conventional way of separately generating electricity and heat [5]. Hence, the mass deployment of EVs alongside grid incorporated CHP and renewable energy sources (RES) can decarbonize the power distribution network and contribute to the electrification of the transport sector. However, EVs currently constitute a small but rapidly expanding part of the transport market. Notwithstanding, EVs are promising substitutes for fossil fuel drivetrains as they offer more carbon benefits than ICEs. They do not produce tank-to-wheel GHGs and have higher tank-to-wheel efficiency than other drivetrains. In addition, EVs can shape power demand curves during on-peak or off-peak periods. [6,7] discussed the optimal deployment of grid-to-vehicle (G2V) and vehicle-to-grid (V2G) infrastructures in reconciling the differential gap in power supply and demand, minimizing charging, and discharging costs, reducing GHG emissions and maximizing the profits of EV owners. Furthermore, the incorporation of small-scale distributed CHP technologies, photovoltaic (PV) systems, wind turbines (WT), fuel cells and battery energy storage systems (BESS) into the existing power distribution network offers the advantages of achieving lower operating costs, reduced CO_2 emissions and network reinforcement in aiding the flexible G2V and V2G operations of EV [8].

Moreover, an essential factor to evolve towards a cleaner and cost-effective energy system is to develop multi-energy system (MES). A MES can feature better technical, economic and environmental performance relative to independent energy systems. A MES has multiple terminal resources and multiple distributed components for energy generation, conversion, and storage. Therefore, a networked energy system with optimized multi-energy resources can be designed [9]. By taking into account the MES districts, recent studies have indicated that distributed generation (DG) can provide major advantages by integrating complementary technologies such as harmonized natural gas and fuel cell CHP units. In fact, they can locally generate electricity and heat, while significantly decreasing operating costs, thus offering enhanced flexibility in supplying the electricity grid [10,11]. Hence, this paper aims to achieve these stated merits using a decentralized novel approach that will support EVs' mass use and contribute to decarbonizing the transport sector in a MES framework.

1.2. Literature review

Many studies have been conducted on the design and operation of CHP systems. Most of these studies have focused on establishing an integrated system among diverse energy sectors. Authors in [12–15] have designed the CHP system on the basis of proton exchange membrane fuel cells (PEMFC) integrated with methanol-reforming and dehumidification to supply electricity/thermal demand, enhance the utilization of RES, and reduce the energy consumption and environmental pollution. Also, the effects of operating parameters of PEMFC and refrigeration system on the energy, exergy, economy and environment are studied over a multi-objective optimization approach. Furthermore, the ongoing energy transition has led to diverse research in the electrification of road transport to address its impact on the environment and achieve the global Net-Zero targets. According to [16–18], EVs will play a principal role in attaining the Net-Zero targets due to their higher energy efficiency and ability to use energy from RESs for G2V operations. Also, when connected to the power distribution network, EVs could support the grid (V2G operations), balance supply and demand, and thus, facilitate the incorporation of RESs. Nevertheless, the authors in [16–18] did not give much attention to reducing CO_2 emissions. Also, the authors did not consider strategies of lowering the operating costs and analysing the uncertainties.

The cost-optimization method suggested by [19–21] uses the optimal scheduling of EV charging as a means to lower the overall cost of the system, reduce network losses and enhance power quality. These optimization approaches explored the use of global and local optimization methods, smart meters and optimal placement of the charging points at different sections of the power network. However, while these studies offered some operating costs reduction, they failed to consider the environmental implications of the widespread of EVs on the existing electricity grid and deploy small scale carbon-free or low carbon distributed generation sources to support the existing grid and minimize GHG emissions. A more comprehensive approach, such as that seen in the [22] study, implemented a multi-objective techno-economic environmental optimization model to concurrently reduce the electricity running cost, carbon dioxide emissions, grid utilization and EVs' battery degradation. Although the authors extensively highlighted the economic and environmental benefits of EVs' deployment in [19–22], they did not take into account the integration of highly efficient CHP technologies and multi-RES in reinforcing the power distribution network. Also, they did not consider the uncertainty of the renewable generations and load consumption.

Authors in [23] have investigated the optimal sizing of a hybrid PV-battery-diesel system in curtailing the overall costs of EVs in a V2G enabled parking lot. The authors applied a heuristic optimization approach in deciding the optimal size of the hybrid system, which led to a 5.21% reduction in the system's overall cost. But the CO_2 benefit of this system was not analysed, and the achieved cost minimization is a bit low when compared with other related studies. [24] explored the addition of hybrid solar-wind energy sources with the distribution network to reduce the computational cost of the optimal power flow calculations in EV charging operations. The authors employed a parallel epsilon variable multi-objective genetic algorithm to solve the probabilistic optimal power flow, and the results obtained validated the effectiveness of the proposed method. Furthermore, a concession of 30.13% and 16.94% in load peak-to-valley and standard deviation were achieved by [25] research exploring the orderly scheduling of EV charging using deep learning. The authors combined the convolutional neural network and deep belief network, which they termed CNN-DBN, to predict the load demand and outputs of the RESs required to charge the EVs while lowering the distribution network's operating costs. In this framework, the network's economic aspect is considered, while the integration of BESS and distributed CHP technologies to reduce CO_2 emissions and operational costs were not examined. Similarly, [26] proposed an integrated Grey Wolf Optimizer and Taguchi test method as a promising approach for minimizing microgrid procurement costs, reducing power losses and CO_2 emissions of the distribution network to aid the extensive use of EVs. The writers tested the adequacy of this method on a modified IEEE 69-bus system to justify the recommended approach. Although the uncertain parameter are considered in the operation problem, research pieces in [23–26] failed to employ a BESS to support the V2G operations in meeting power demand at peak demand periods. Furthermore, [27] investigated the co-location of CHP units for the fast charging of EVs, which is crucial in encouraging the mass use of EVs, as it addresses the concern on EV prolong charging. The authors analysed three different CHP configurations to find the most fuel-efficient strategy, explored the charging behaviour of EV drivers and showcased the advantage of variable speed generators over fixed speed counterpart in lowering the CHP's fuel consumption. However, they failed to inspect the CO_2 impact of the CHP unit or consider a fuel cell CHP strategy to curb the system's environmental footprints. Besides, they did not take into account the uncertainties of the system.

Table 1 provides a summarized view of the previous papers within the research focus and their various limitations. Some research gaps (RG) recognized in the reviewed literature can be mentioned as follows:

RG1: The economic and environmental analysis of V2G facility and CHP technology in supporting the existing power distribution network, lowering CO_2 emissions, and minimizing the operating costs were not explicitly proposed in a stochastic framework.

RG2: The integration of BESS and RESs to support V2G facility and CHP technology during peak load hours and minimize the wastage of excess power from the CHP units are not taken into account in the reviewed papers.

RG3: Previous works did not take any additional measures to lower the carbon footprints of the grid integrated CHP technologies to decarbonize its operations and minimize the overall CO_2 emission of the system.

1.3. Research contributions

The electricity and transport sectors are getting increasingly connected. Hence, most of the energy for charging EVs will come from the national electricity grid, which is currently dominated by high operational expenses and large fossil fuel-driven power plants. Therefore, this paper focuses on minimizing the power distribution network's operating and CO_2 emissions costs in aiding the mass deployment of EVs. It examines the integration of harmonized natural gas and fuel cell CHP technologies, PVs arrays, WTs, and BESS in a stochastic energy management of the existing power distribution network. Furthermore, it investigates the benefits of operating V2G and G2V strategies in the

Table 1
A comparative summary of previous papers and this research.

Ref.	Uncertain parameters			Objective function		Operation units				
	Load	RES	EV	CO_2 emission	Operating cost	CHP unit	Fuel cell	RES	BESS	V2G
[16]	✖	✖	✖	✓	✖	✖	✖	✓	✖	✖
[17]	✖	✖	✖	✓	✖	✖	✖	✓	✖	✖
[18]	✖	✖	✖	✓	✖	✖	✖	✓	✖	✖
[19]	✖	✖	✖	✓	✓	✖	✖	✖	✖	✓
[20]	✖	✖	✓	✓	✓	✖	✖	✖	✖	✓
[21]	✖	✖	✖	✓	✓	✖	✖	✖	✖	✖
[22]	✖	✖	✖	✓	✓	✖	✖	✓	✖	✓
[23]	✖	✓	✖	✓	✓	✖	✖	✓	✓	✓
[24]	✓	✓	✓	✓	✓	✖	✖	✓	✖	✖
[25]	✓	✓	✓	✓	✓	✖	✖	✓	✖	✖
[26]	✖	✓	✖	✓	✓	✓	✖	✓	✖	✓
[27]	✖	✖	✖	✓	✓	✓	✖	✓	✖	✖
This paper	✓	✓	✓	✓	✓	✓	✓	✓	✓	✓

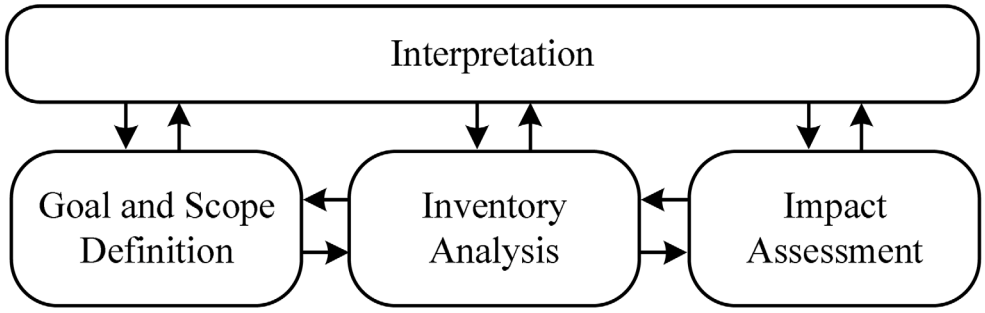

Fig. 1. Life cycle assessment framework.

power network. For the sake of a detailed analysis of the CO_2 emissions, the life cycle assessment (LCA) is also calculated.

Based on the mentioned RGs in the reviewed pieces of literature, the following research contributions (RC) are made:

RC1: Employ an hourly cost-effective-based G2V and V2G strategies to support the electricity grid network, facilitate peak shaving in high power demand periods, and act as an on-demand carbon-free energy source (Addresses **RG1**).

RC2: Investigate the economic and environmental contributions of BESS in aiding V2G and G2V facilities, reducing wastage of excess power, minimizing CO_2 emissions, and lowering the overall operating costs of power network and EV owners (Addresses **RG2**).

RC3: Model and formulate a harmonized natural gas and fuel cell CHP system following the hybrid electric-thermal strategy. Besides, integrate a natural gas fuel reformer with the CHP technology to provide the hydrogen required to operate the fuel cell units in the harmonized CHP system, thus, reducing the carbon footprints of the CHP output. (Addresses **RG3**).

2. Model and problem formulation

2.1. Life cycle assessment

LCA includes four stages, goal and scope definition, life cycle inventory analysis, life cycle impact assessment and interpretation. These stages are summarized in Fig. 1 for a proper illustration [28].

To explain briefly each stage; goal and scope definition enables the system operator to determine the goal of the proposed research, to set physical and dimensional system limitations, and to determine which type of LCA to utilize. The inventory analysis is commonly the most work intensive stage and contains collecting of life cycle inventory data for all foundations modelled processes and integration of those data into the greater model. Impact assessment implies calculation of emissions and impacts. In the interpretation stage, the system operator analyses the outcomes of the impact assessment, and may select from a variety of interpretation implements to support this analysis. There is continual feedback among the diverse stages, as shown by the arrows in Fig. 1, as data disclosed in various stages affects decisions and outcomes in preceding and subsequent stages [29].

Environmental life cycle impact categories associate to atmospheric, aquatic and terrestrial impacts due to material release or exhaustion in the environment. The global warming potential is the major recognized environmental impact category influencing the net zero GHG strategies. In this paper, the mathematical equations and approaches for environmental LCA of DERs including PV, WT, and CHP unit are defined. For the brevity of the LCA model of this paper, its scope has been confined to the analysis at the global warming potential (amount of CO_2eq). The environmental life cycle impact characterization of a material in an impact category is the alteration in its fundamental property responsible for the category due to alteration in its plenty in the environment with respect to the alteration of a reference material as demonstrated in Eq. (1).

$$LCIA_{j=y,k} = \frac{\int_0^{TH} a_{j=y,k} y(t)dt}{\int_0^{TH} a_{j=y,k} r(t)dt} \tag{1}$$

$LCIA_{j=y,k}$ is the life cycle impact characterization of a material y in an impact category k. $a_{j,k}$ is the fundamental property increase of the material y or relative material r for its unit application alternation in the environment. The function of time $y(t)$ is the alternation in plenty due to prompt release or exhaustion of the material. TH is the period of the computation. As the life cycle impact characterization of a material in an impact category is the ratio with respect to a reference material, the unit of life cycle impact characterization of a material is mass of the reference material equal. An absolute environmental impact in a category E_k can be calculated applying Eq. (2).

$$E_k = \sum_j LCIA_{j,k} \times m_j \tag{2}$$

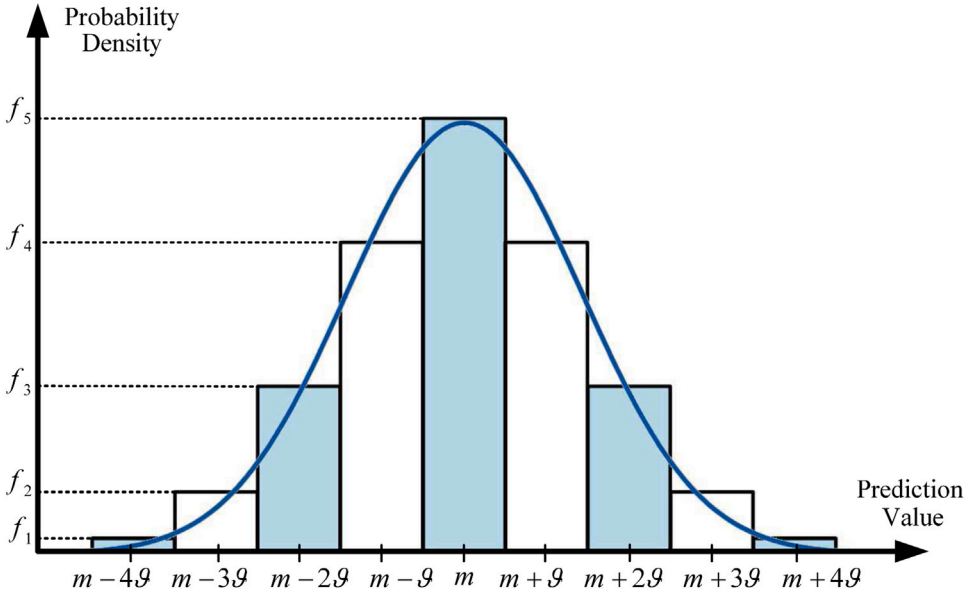

Fig. 2. Normal probability distribution function related to the standard deviation of prediction.

where, m_j is the quantity or inventory of the pollutant j emitted to the environment [30].

2.2. Scenario-based analysis for modelling uncertainty

As the RES generations, the load consumption, and the behaviour patterns of charging/discharging periods of EVs are uncertain and stochastic, employing a deterministic framework will not guarantee a thorough insight into the potential benefits of integrating distributed energy resources [31]. To properly handle the uncertainties, a scenario-based analysis (SBA) is used to generate the number of scenarios as well as a backward scenario reduction strategy to decrease them. More details on the scenario reduction strategy can be found in [32]. In SBA method, the Probability Density Function (PDF) curve of the uncertain parameter is divided into multiple levels. Applying the PDF, the probability of the uncertain variable in each level can be calculated. Stochastic framework is modelled in this paper as a normal Gaussian PDF, where the mean is equal to the forecasted value. In major samples, the forecasted value is considered as the standard deviation of PDF. The formulation of the normal Gaussian PDF is presented as Eqs. (3).

$$f(x|m,\vartheta^2)=\frac{1}{\sqrt{2\pi\vartheta^2}}\exp\left(-\frac{(x-m)^2}{2\vartheta^2}\right),\quad -\infty<x<+\infty \tag{3}$$

where x indicates the uncertain parameter, m is the mean of the forecasted input variable, ϑ^2 is the variance and ϑ is the standard deviation of the forecasted input variable. Fig. 2 demonstrates the normal PDF divided into multiple segments with diverse probability levels [33].

2.3. Modelling a harmonized natural gas and fuel cell CHP system

Fig. 3 presents the single line diagram of the harmonized natural gas and hydrogen fuel cell CHP technologies, which are modelled following the hybrid electric-thermal strategy. The mathematical models are a function of the amount of natural gas supplied to the power generation unit (PGU) and the fuel reformer. Hence, the efficiency of the PGU is expressed as Eq. (4).

$$\eta_{\mathrm{PGU}}=\frac{E_{\mathrm{PGU}}}{N_{\mathrm{PGU}}} \tag{4}$$

where E_{PGU} is the total electricity (kWh) derived from the power generation unit, and N_{PGU} is the natural gas consumed by the PGU. Also, the efficiency of the PGU is assumed constant and is independent of the electric load demand.

Similarly, the efficiency of the fuel reformer and fuel cell unit are determined Eqs. (5) and (6), respectively.

$$\eta_{\mathrm{FR}}=\frac{H_{\mathrm{FR}}}{N_{\mathrm{FR}}} \tag{5}$$

$$\eta_{\mathrm{FCU}}=\frac{E_{\mathrm{FCU}}}{H_{\mathrm{FCU}}} \tag{6}$$

where H_{FR} and N_{FR} are the hydrogen from the fuel reformer and natural gas consumed by the fuel reformer, respectively. E_{FCU} is the electricity generated by the fuel cell unit and H_{FCU} is the hydrogen consumption of the unit.

In addition, the fuel reformer and fuel cell unit efficiencies are constant and are independent of the heat load and electric load, respectively. Therefore, the hydrogen from the fuel reformer is equal to the hydrogen inputted into the fuel cell unit. Hence, Eqs. (7) and (8) can be obtained from Eqs. (5) and (6) [34].

$$H_{\mathrm{FR}}=\eta_{\mathrm{FR}}\times N_{\mathrm{FR}}=H_{\mathrm{FCU}} \tag{7}$$

$$E_{\mathrm{FCU}}=\eta_{\mathrm{FCU}}(\eta_{\mathrm{FR}}\times N_{\mathrm{FR}}) \tag{8}$$

The by-product heat recovered from the PGU and passed through the heat recovery unit can be estimated as the difference between the PGU natural gas consumption and the electricity produced by the PGU, multiplied by the efficiency of the heat recovery unit as demonstrated in Eq. (9) [34].

$$Q_{\mathrm{PGU}}=(N_{\mathrm{PGU}}-E_{\mathrm{PGU}})\times\eta_{\mathrm{HRU}} \tag{9}$$

where Q_{PGU} is the recovered heat from the PGU and η_{HRU} is the efficiency of the heat recovery unit. By substituting Eq. (4) into Eq. (9), Eq. (10) is obtained.

$$Q_{\mathrm{PGU}}=N_{\mathrm{PGU}}(1-\eta_{\mathrm{PGU}})\times\eta_{\mathrm{HRU}} \tag{10}$$

Correspondingly, the heat recovered from the fuel reformer and into the heat recovery unit can be approximated as Eq. (11).

$$Q_{\mathrm{FR}}=(N_{\mathrm{FR}}-H_{\mathrm{FR}})\times\eta_{\mathrm{HRU}}=(N_{\mathrm{FR}}-\frac{E_{\mathrm{FCU}}}{\eta_{\mathrm{FCU}}})\times\eta_{\mathrm{HRU}} \tag{11}$$

Also, by substituting Eq. (8) into Eq. (11), Eq. (12) is obtained.

$$Q_{\mathrm{FR}}=[N_{\mathrm{FR}}-\frac{\eta_{\mathrm{FCU}}(\eta_{\mathrm{FR}}\times N_{\mathrm{FR}})}{\eta_{\mathrm{FCU}}}]\times\eta_{\mathrm{HRU}}=N_{\mathrm{FR}}[1-\frac{\eta_{\mathrm{FCU}}\times\eta_{\mathrm{FR}}}{\eta_{\mathrm{FCU}}}]\times\eta_{\mathrm{HRU}} \tag{12}$$

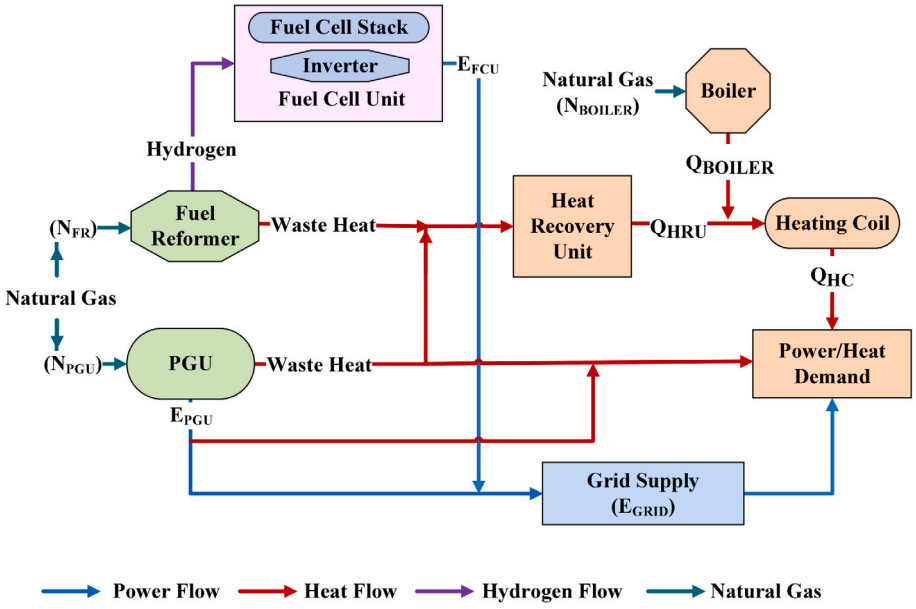

Fig. 3. Schematic of a harmonized natural gas and fuel cell CHP system.

where Q_{FR} is the heat recovered from the fuel reformer. Thus, the amount of heat recovered from the power generation unit and the fuel reformer depends on the amount of natural gas they consume. The recovered heat passing through the heat recovery unit is then stated as as Eq. (13).

$$Q_{HRU} = Q_{PGU} + Q_{FR} \tag{13}$$

From Eqs. (4) and (10), the electricity produced by the PGU can be written as as Eq. (14).

$$E_{PGU} = \frac{\eta_{PGU}}{(1-\eta_{PGU})\times\eta_{HRU}} Q_{PGU} \tag{14}$$

Also, using Eqs. (8) and (12), the electricity produced by the fuel cell unit is expressed as as Eq. (15):

$$E_{FCU} = \frac{\eta_{FCU}\times\eta_{FR}}{(1-\frac{\eta_{FCU}\times\eta_{FR}}{\eta_{FCU}})\times\eta_{HRU}} Q_{FR} \tag{15}$$

Since the expressions multiplied by the variables Q_{PGU} and Q_{FR} comprise of only constant variables, they can be expressed as new constant K_{PGU} and K_{FCU}, as presented in Eqs. (16) and (17), respectively.

$$K_{PGU} = \frac{\eta_{PGU}}{(1-\eta_{PGU})\times\eta_{HRU}} \tag{16}$$

$$K_{FCU} = \frac{\eta_{FCU}\times\eta_{FR}}{(1-\frac{\eta_{FCU}\times\eta_{FR}}{\eta_{FCU}})\times\eta_{HRU}} \tag{17}$$

Thus, Eqs. (14) and (15) can be rewritten as Eqs. (18) and (19), respectively.

$$E_{PGU} = (K_{PGU})Q_{PGU} \tag{18}$$

$$E_{FCU} = (K_{FCU})Q_{FR} \tag{19}$$

From Eqs. (18) and (19), it is clear that the electricity generated by the CHP system is a linear function of the heat recovered. Hence, the total electricity produced by the harmonized natural gas and fuel cell CHP system following the hybrid electric-thermal strategy is then determined as demonstrated in Eq. (20).

$$E_{total}^{CHP} = E_{PGU} + E_{FCU} = (K_{PGU})Q_{PGU} + (K_{FCU})Q_{FR} \tag{20}$$

Using the above linear equations, a perfect match between the electrical and thermal loads can be found [35]. However, due to the fluctuation in the energy required by the electrical load (EVs and buildings) and the buildings' heat demands, it is difficult to continuously match both the electricity and heat demands. Therefore, to reduce the excess electricity or heat generated by the CHP, avoid wastage and minimize unwarranted CO_2 emissions, the CHP system operating in the hybrid electric-thermal load strategy is designed to autonomously follow the best optimal operations by switching between following electrical load demand (FELD) and following thermal load demand (FTLD) strategies.

For $E_{req} < (K_{CHP})Q_{req}^{bulding}$, the FELD strategy will be followed for the CHP system. Also, for $E_{req} > (K_{CHP})Q_{req}^{bulding}$, the FTLD strategy will be selected. E_{req} is the electricity required by the EVs and buildings. Furthermore, (K_{CHP}) represents a constant coefficient. While $Q_{req}^{bulding}$ is the heat required to meet the building's heat load. Therefore, the electricity generated by the harmonized CHP system can be determined as Eqs. (21) and (22).

$$\text{if } E_{req} < (K_{CHP})Q_{req}^{bulding},\ E_{total}^{CHP} = E_{req} \tag{21}$$

$$\text{if } E_{req} > (K_{CHP})Q_{req}^{bulding},\ E_{total}^{CHP} = E' = (K_{CHP})Q_{req}^{bulding} \tag{22}$$

Using Eqs. (21) and (22), the heat captured by the heat recovery unit can be expressed as Eqs. (23) and (24).

$$\text{if } E_{req} < (K_{CHP})Q_{req}^{bulding},\ Q_{HRU} = Q' = \frac{E_{total}^{CHP}}{K_{CHP}} \tag{23}$$

$$\text{if } E_{req} < (K_{CHP})Q_{req}^{bulding},\ Q_{HRU} = Q_{req}^{bulding} \tag{24}$$

When the CHP switches to the FELD strategy mode ($E_{req} < (K_{CHP})Q_{req}^{bulding}$), an auxiliary boiler ($Q_{BOILER}$) supplies the supplementary heat required by the buildings as in Eq. (25).

$$Q_{BOILER} = Q_{req}^{bulding} - Q' = Q_{req}^{bulding} - \frac{E_{req}}{K_{CHP}} \tag{25}$$

Also, when the CHP switches operation to the FTLD strategy mode ($E_{req} > (K_{CHP})Q_{req}^{bulding}$), the additional electricity required to power the buildings and EVs chargers is purchased from the electricity grid (with incorporated RESs) and defined as in Eq. (26).

$$E_{GRID} = E_{req} - E' = E_{req} - (K_{CHP})Q_{req}^{bulding} \tag{26}$$

The total amount of natural gas consumed by the power generation unit, fuel reformer (for hydrogen production) and the auxiliary boiler are denoted in Eqs. (27) and (28) for FELD and FTLD strategies, respectively.

$$\text{FELD}: \quad N_{\text{total}} = N_{\text{PGU}} + N_{\text{FR}} + N_{\text{BOILER}} = \frac{E_{\text{PGU}}}{\eta_{\text{PGU}}} + \frac{E_{\text{FCU}}}{\eta_{\text{FCU}} \times \eta_{\text{FR}}} + \frac{Q_{\text{BOILER}}}{\eta_{\text{BOILER}}} \tag{27}$$

$$\text{FTLD}: \quad N_{\text{total}} = N_{\text{PGU}} + N_{\text{FR}} = \frac{E_{\text{PGU}}}{\eta_{\text{PGU}}} + \frac{E_{\text{FCU}}}{\eta_{\text{FCU}} \times \eta_{\text{FR}}} \tag{28}$$

where N_{BOILER} is natural gas consumed by the boiler, and η_{BOILER} is the boiler's thermal efficiency. The cost of operating the harmonized CHP system in the hybrid strategy mode is expressed as Eq. (29).

$$\text{cost}_{\text{CHP-FHL}} = (N_{\text{PGU}} + N_{\text{FR}} + N_{\text{BOILER}}) \times \text{cost}_{\text{NG}} + E_{\text{GRID}} \times \text{cost}_{\text{elect}} \tag{29}$$

where E_{GRID} is the electricity purchased from the grid. While cost_{NG} and $\text{cost}_{\text{elect}}$ are the cost of the natural gas and grid electricity, respectively. Also, the amount of carbon dioxide emitted by the CHP system is determined as Eq. (30).

$$\text{CD}_{\text{Emission}} = (N_{\text{PGU}} + N_{\text{FR}} + N_{\text{BOILER}}) \times \gamma_{\text{NG}} + E_{\text{GRID}} \times \gamma_{\text{GRID}} \tag{30}$$

where γ_{NG} and γ_{GRID} are the emission conversion factor of the natural gas and grid, respectively. Fig. 4 presents the flowchart of the harmonized natural gas and fuel cell CHP system following the hybrid electric-thermal strategy [34].

2.4. Modelling of G2V and V2G facilities of EVs

The modal of EV is indicated by Eqs. (31)–(37). The default charging and discharging periods of EVs to investigate the desired facilities of G2V and V2G can be as follows in Eqs. (31) and (32). These periods can be changed based on the generated scenarios.

$$T_{\text{Ch}}^{\text{Day}} = \{1, 2, \ldots, 6\} \Rightarrow \text{G2V operation} \tag{31}$$

$$T_{\text{Dch}}^{\text{Day}} = \{18, 19, \ldots, 24\} \Rightarrow \text{V2G operation} \tag{32}$$

where T_{Charge}^{Day} and $T_{Discharge}^{\text{Day}}$ are the time of day in hours that EVs allowed to be charge or discharge. In other words, the arrival and departure times of EVs in the charging station are related to their charging and discharging times. The energy balance of EV batteries is formulated by Eq. (33).

$$\text{SOC}_t^{\text{EV}} = \text{SOC}_{t-1}^{\text{EV}} + \left(P_t^{\text{EV+}}.\eta^{\text{EV-}} - P_t^{\text{EV-}}/\eta^{\text{EV-}}\right)/P_{\text{Total}}^{\text{EV}} \tag{33}$$

where SOC_t^{EV} is the EV's battery state of charge (SoC) at time t, $P_t^{\text{EV+}}$ and $P_t^{\text{EV-}}$ are the charging and discharging energies in the EV battery at time t, respectively, and $P_{\text{Total}}^{\text{EV}}$ is the total energy that can be stored in the EV battery (EV battery capacity). At any given time, the SoC of EV batteries must be in its allowed capacity as shown in Eq. (34).

$$\underline{SOC}^{\text{EV}} \le \text{SOC}_t^{\text{EV}} \le \overline{SOC}^{\text{EV}} \tag{34}$$

where $\underline{SOC}^{\text{EV}}$ and $\overline{SOC}^{\text{EV}}$ are the minimum and maximum SoC of the EV battery, respectively. Eqs. (35) and (36) demonstrate the upper/lower limits of charging/discharging of EV battery.

$$0 \le P_t^{\text{EV+}} \le P_{\text{Total}}^{\text{EV}}.\left(1 - \text{SOC}_{t-1}^{\text{EV}}\right)/\eta^{\text{EV+}} \tag{35}$$

$$0 \le P_t^{\text{EV-}} \le P_{\text{Total}}^{\text{EV}}.\text{SOC}_{t-1}^{\text{EV}}.\eta^{\text{EV-}} \tag{36}$$

Besides, each EV should be charged to its targeted SoC during the departure period (charging period) as represented by Eq. (37) [36].

$$\text{SOC}_{t\text{Dep}}^{\text{EV}} = \text{SOC}^{\text{EV, Dep}} \tag{37}$$

2.5. Modelling wind turbine

The effective power produced by the wind turbine to feed into the MG network can be estimated based on Eqs. (38)–(40).

$$P_{\text{eff}}^{\text{WT}} = 1/2 \times (\eta_{\text{WT}} \cdot \rho \cdot A \cdot \overline{C}^3) \tag{38}$$

$$\eta_{\text{WT}} = C_p \cdot \eta_{\text{gear}} \cdot \eta_{\text{gen}} \eta_{\text{elec}} \tag{39}$$

$$A = \pi \cdot [(l_{\text{WT}} + r_{\text{WT}})^2 - (r_{\text{WT}})^2] = \pi \cdot l_{\text{WT}}(l_{\text{WT}} + 2 \cdot r_{\text{WT}}) \tag{40}$$

where ρ is the density of air, A is the swept area of the wind turbine blades, $\overline{C}$ is the average wind speed over a specified period, C_p is the power coefficient, while η_{gear}, η_{gen} and η_{elec} are the efficiency of the gearbox, generator, and electric components, respectively. l_{WT} is the length of the wind turbine blades, and τ_{WT} is the wind turbine hub's radius. In addition, the wind speed variation at the selected wind turbine site can be described using the Weibull distribution function [37]. Hence, the probability density function of the Weibull variable $\overline{C}$ is defined as Eq. (41).

$$f(\overline{C}, k, \lambda) = \begin{cases} \frac{k}{\lambda}(\frac{\overline{C}}{\lambda}) \cdot \exp(-(\frac{\overline{C}}{\lambda})^k) & \overline{C} \ge 0 \\ 0 & \overline{C} < 0 \end{cases} \tag{41}$$

where k and λ are the shape factor and scale factor, respectively. The shape factor measures the width of the distribution, while the scale factor relates closely to the average wind speed. The value of the Weibull's shape factor (k) and Weibull's scale factor (λ) changes with respect to the selected site's wind profile [38].

2.6. Modelling PV arrays

The power produced by the PV panels is defined as Eq. (42).

$$P_t^{\text{PV}} = \frac{E_t^{\text{PV}}}{t} = \frac{N_{\text{Total}}^{\text{PV}} \times A \times \eta \times H \times \text{PR}}{t} \tag{42}$$

where $N_{\text{Total}}^{\text{PV}}$ is the total number of PV panels, A is the area of each PV panel, η is the PV panel's efficiency, H is the amount of solar radiation hitting the panel, and PR is the panel's performance ratio or coefficient losses. Also, the temperature of the panels and the average energy produced by the PV arrays can be estimated based on Eqs. (43) and (44).

$$T^{\text{panel}} = T^{\text{amb.}} + \frac{(N_{\text{OT}} - 20)}{0.8} \times H \tag{43}$$

$$E_{\text{av.}}^{\text{PV}} = N_{\text{Total}}^{\text{PV}} \times (A \times \eta \times H \times \text{PR}) \tag{44}$$

where T^{panel} and $T^{\text{amb.}}$ are the temperature of the panel and ambient temperature, respectively [39].

2.7. Modelling BESS

The incorporated BESS in this design reinforces the RESs due to their intermittent nature, stores the excess electrical energy from the CHP technologies, and supports V2G operations during peak demand periods. In addition, the BESS is optimized to save MG's operating costs and lower CO_2 emissions. Hence, the system stores electrical energy when electricity price and CO_2 emission rates are low, and discharges to meet high demand prices and minimize CO_2 emissions. At any given time, the SOC of BESS should be in its determined limits as indicated in Eq. (45).

$$\underline{\text{SOC}}^{\text{BESS}} \le \text{SOC}_t^{\text{BESS}} \le \overline{\text{SOC}}^{\text{BESS}} \tag{45}$$

where $\text{SOC}_t^{\text{BESS}}$ is the BESS state of charge at time t, $\underline{\text{SOC}}^{\text{BESS}}$ and $\overline{\text{SOC}}^{\text{BESS}}$ are the minimum and maximum state of charge of the BESS,

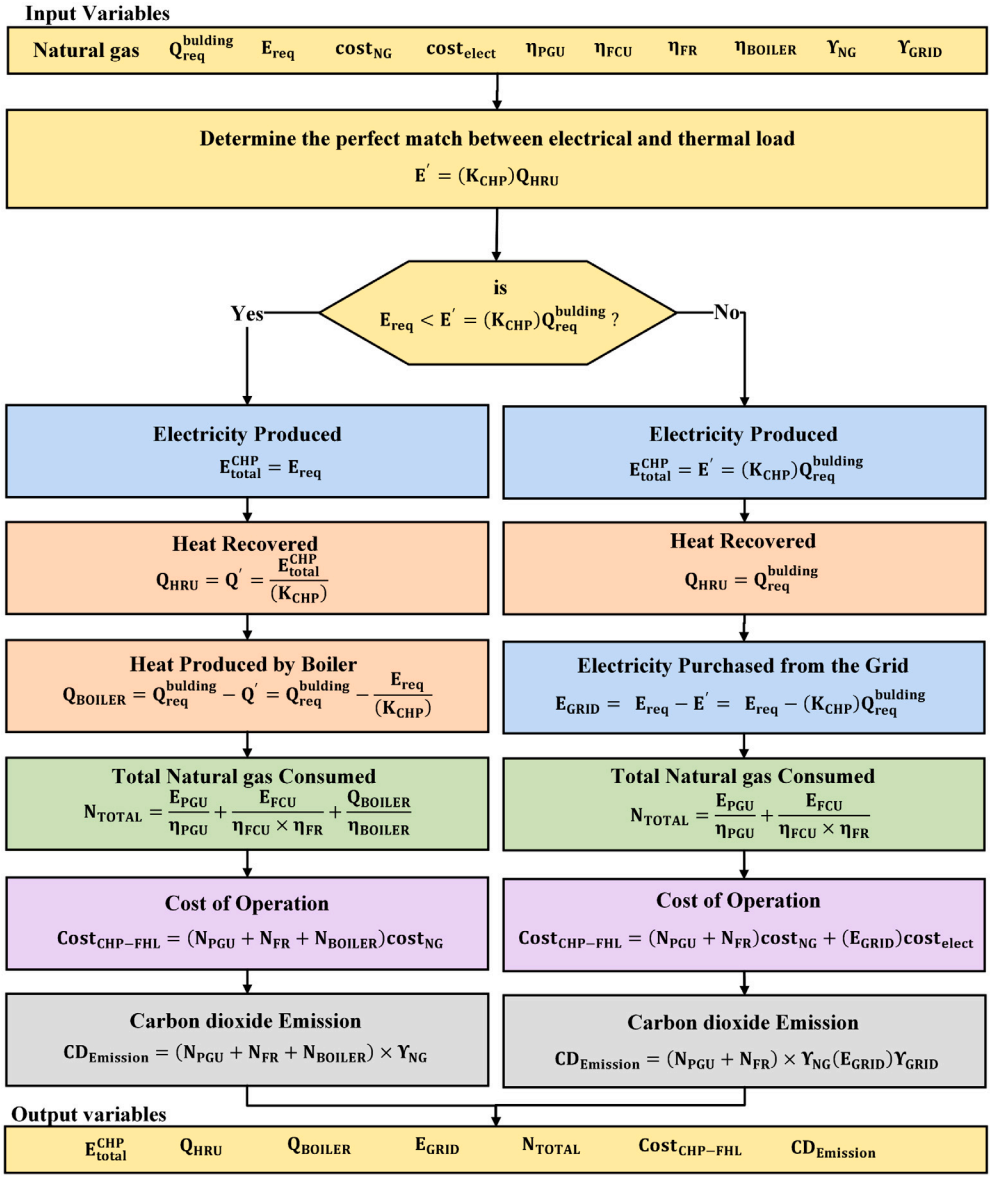

Fig. 4. Flowchart of a harmonized natural gas and fuel cell CHP system following the hybrid electric-thermal strategy.

respectively. The maximum power required to charge the BESS can be defined as Eq. (46).

$$\overline{P}_t^{BESS+} = \frac{(SOC_t^{BESS} - \underline{SOC}^{BESS}) \times E_{Total}^{BESS}}{t} > 0 \quad (46)$$

E_{Total}^{BESS} is the total electrical energy that can be stored in the BESS [40].

2.8. Modelling MG power demand

The MG network design consists of CHP technologies, WT, PV arrays, and BESS integrated into the power distribution network to support EVs' G2V and V2G operations as well as the power demand. The power balance formulation can be expressed as Eq. (47).

$$P_t^{EV+} - P_t^{EV-} = P_t^{CHP} + P_t^{PV} + P_t^{WT} + P_t^{BESS-} - P_t^{BESS+} + P_t^{grid-} - P_t^{grid+} - P_t^{Load} \quad (47)$$

where P_t^{EV+} and P_t^{EV-} are the power required to charge the EVs and power discharge to the grid at time t, respectively. P_t^{CHP}, P_t^{PV}, P_t^{WT} are the power produced by the CHP, PV and WT, respectively. P_t^{BESS-} and P_t^{BESS+} are the discharge and charge power of the BESS, respectively. Also, P_t^{grid-} and P_t^{grid+} are indicates the power purchased from the electricity grid and power sell to the electricity grid, respectively. P_t^{Load} is the power demand of the MG. If P_t^{Load} is assumed to be zero, four operation schemes can be considered in meeting the EVs' power demand.

Scheme 1: The power produced by the CHP, PV and WT meets the EVs' power demand as shown in Eqs. (48) and (49).

$$P_t^{EV+} = (P_t^{CHP} + P_t^{PV} + P_t^{WT}) \quad (48)$$

$$P_t^{BESS} \pm = 0, \quad P_t^{grid} \pm = 0 \quad (49)$$

Scheme 2: The power produced by CHP, PV and WT exceeds the EVs' power demand as shown in Eq. (50).

$$P_t^{EV+} < (P_t^{CHP} + P_t^{PV} + P_t^{WT}) \quad (50)$$

when:

$$E_t^{BESS} < E_{Total}^{BESS} \text{ and } \overline{P}^{BESS+} \geq (P_t^{CHP} + P_t^{PV} + P_t^{WT}) - P_t^{EV+} \quad (51)$$

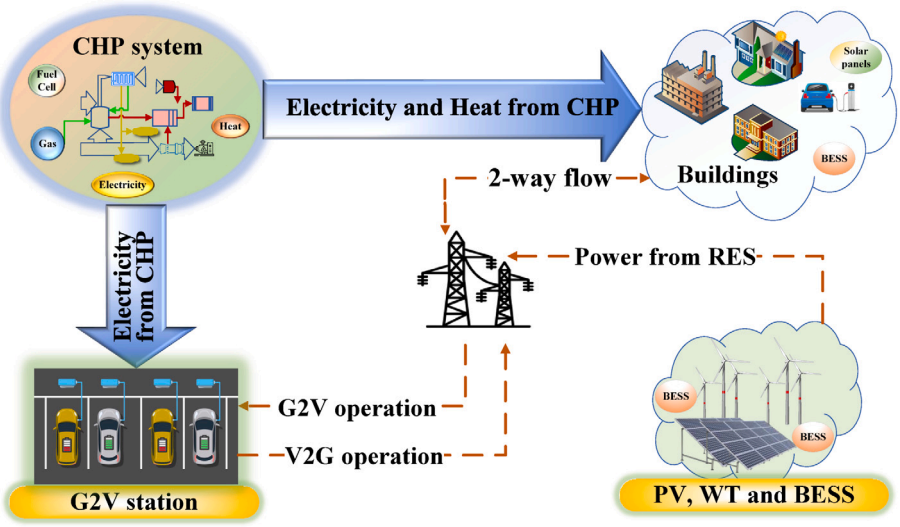

Fig. 5. G2V and V2G operations with CHP technologies, RES, and BESS.

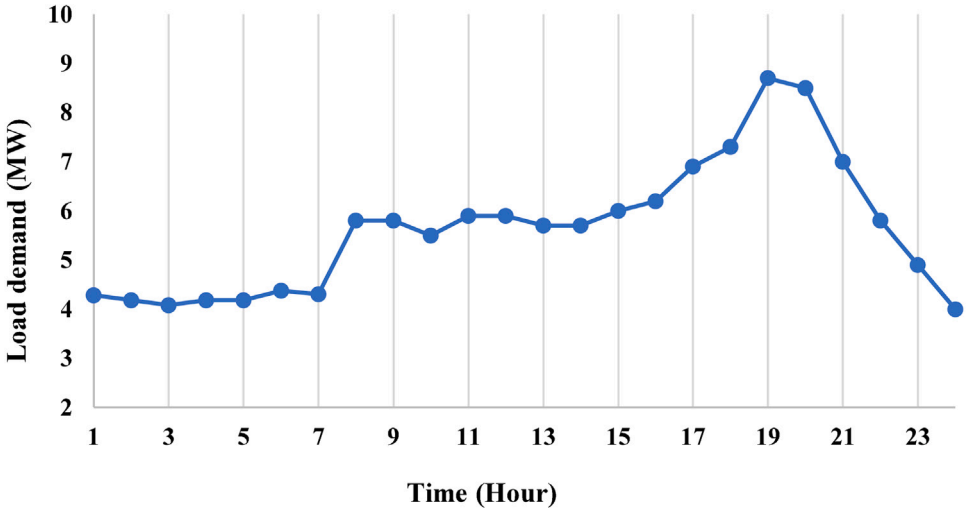

Fig. 6. Hourly average load demand.

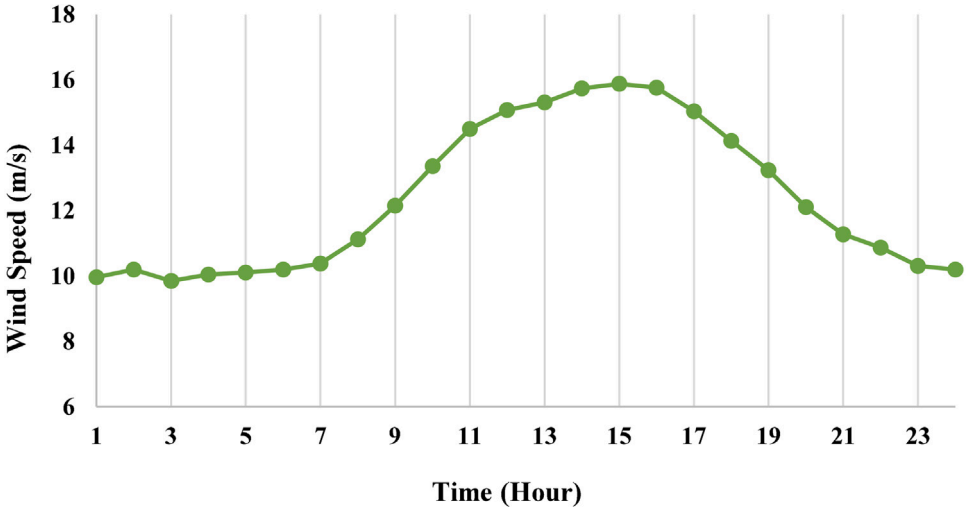

Fig. 7. Hourly average wind speed for North East England.

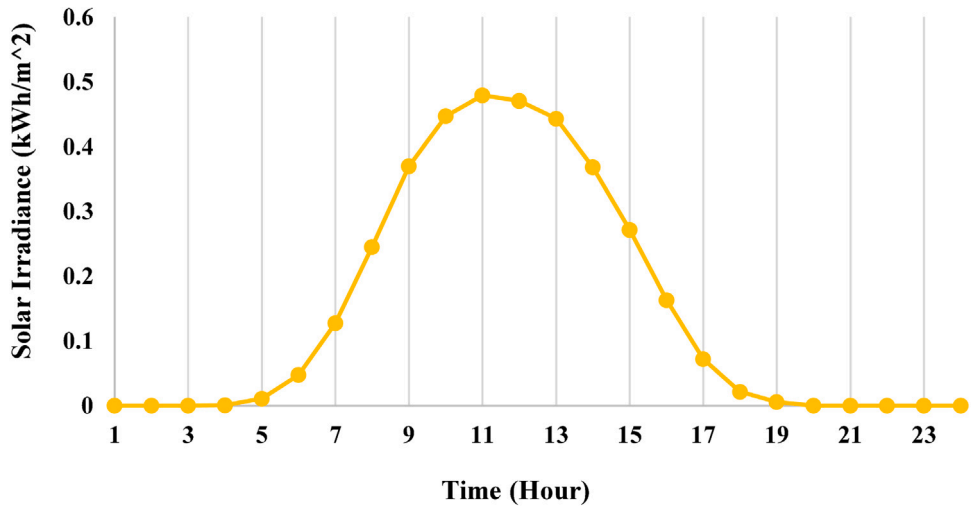

Fig. 8. Hourly average solar irradiance for North East England.

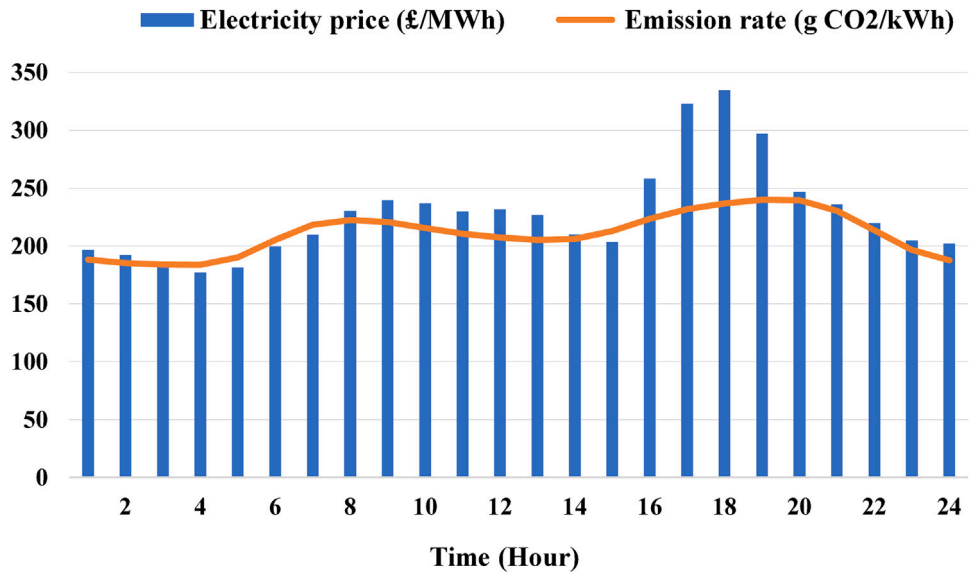

Fig. 9. Hourly electricity prices and CO_2 emission rates for North East England.

Then:

$$P_t^{\text{grid+}} = (P_t^{\text{CHP}} + P_t^{\text{PV}} + P_t^{\text{WT}}) - (P_t^{\text{EV+}} + P_t^{\text{BESS+}}) = 0 \quad (52)$$

$$P_t^{\text{BESS+}} = \frac{\text{SOC}_t^{\text{BESS}} \times E_{\text{Total}}^{\text{BESS}}}{t} \quad (53)$$

Eq. (52) indicates that no power is sold to the grid and Eq. (53) shows the power required to charge the BESS. when:

$$E_t^{\text{BESS}} = E_{\text{Total}}^{\text{BESS}} \quad (54)$$

Then:

$$\text{SOC}_t^{\text{BESS}} = \frac{1}{1} \times 100 = 100\% \quad (55)$$

$$P_t^{\text{grid+}} = (P_t^{\text{CHP}} + P_t^{\text{PV}} + P_t^{\text{WT}}) - (P_t^{\text{EV+}} + P_t^{\text{BESS+}}) > 0 \quad (56)$$

Eq. (54) indicates that BESS is fully charged and Eq. (55) shows the amount of power sold to the grid.

Scheme 3: The power produced by CHP, PV and WT does not meet the EVs' power demand as shown in Eq. (57).

$$P_t^{\text{EV+}} > (P_t^{\text{CHP}} + P_t^{\text{PV}} + P_t^{\text{WT}}) \quad (57)$$

when:

$$\text{SOC}_t^{\text{BESS}} > \underline{\text{SOC}}^{\text{BESS}} \quad (58)$$

Then:

$$\overline{P}_t^{\text{BESS-}} = \frac{\text{SOC}_t^{\text{BESS}} - \underline{\text{SOC}}^{\text{BESS}} \times E_{\text{Total}}^{\text{BESS}}}{t} > 0 \quad (59)$$

Eq. (59) indicates the maximum power supplied by BESS.

when:

$$\text{SOC}_t^{\text{BESS}} = \underline{\text{SOC}}^{\text{BESS}} \text{ or } \overline{P}_t^{\text{BESS-}} < P_t^{\text{EV}} - (P_t^{\text{CHP}} + P_t^{\text{PV}} + P_t^{\text{WT}}) \quad (60)$$

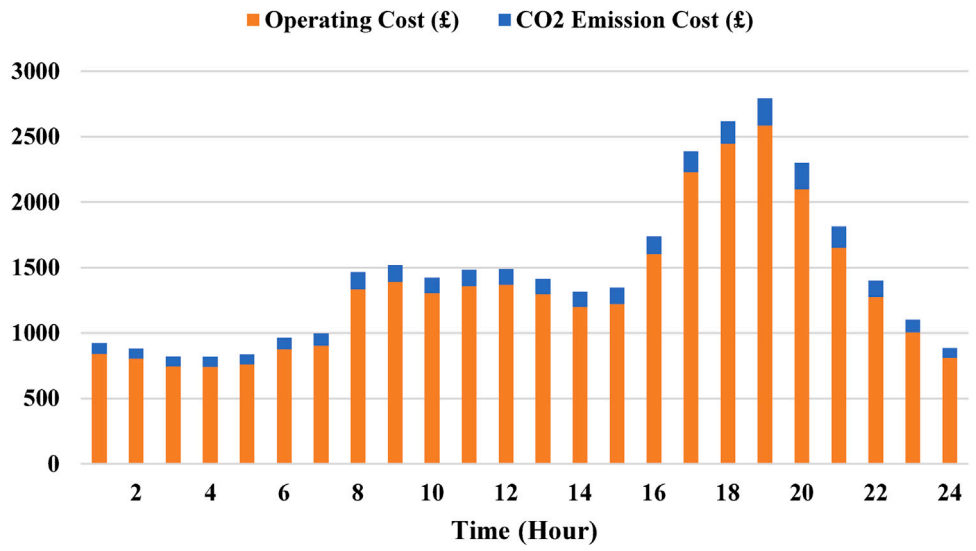

Fig. 10. Operating and CO_2 Emission Costs in **CS0**.

Then:

$$P_t^{\text{grid-}} = P_t^{\text{EV+}} - (P_t^{\text{CHP}} + P_t^{\text{PV}} + P_t^{\text{WT}}) > 0 \tag{61}$$

Eq. (61) shows the amount of power purchased from the grid.

Scheme 4: The power produced by the CHP, PV and WT does not meet the EVs' power demand, and the power purchased from the grid is insufficient. In this scheme, Eqs. (62) and (63) can be presented.

$$P_t^{\text{EV+}} > (P_t^{\text{CHP}} + P_t^{\text{PV}} + P_t^{\text{WT}}) + (\overline{P}_t^{\text{BESS-}} + P_t^{\text{grid-}}) \tag{62}$$

$$P_t^{\text{EPNM}} = \sum P_t^{\text{EV}} - \sum (P_t^{\text{CHP}} + P_t^{\text{PV}} + P_t^{\text{WT}} + P_t^{\text{grid-}} + \overline{P}_t^{\text{BESS-}}) > 0 \tag{63}$$

Eq. (62) indicates that the system has power deficit and Eq. (63) shows the amount of expected power not met [41].

3. Objective functions and constraints

The objective function aims to minimize the operating costs and CO_2 emissions in the MG connected network's G2V and V2G operations of EVs as shown in Eq. (64).

$$\min \ \text{OB}_{\text{function}} = \sum_s \mu_s \left[\text{OP}_{\text{cost}} + (\lambda^{\text{CO}_2})\text{CD}_{\text{emission}}\right] \tag{64}$$

where OP_{cost} is the operating cost function and $\text{CD}_{\text{emission}}$ is the emission function. μ_s is the probability of scenario s. To equalize the dimensions of these two items within the objective function, the price of CO_2 emissions per kg, λ^{CO_2}, is multiplied by the emission function [42].

3.1. Operating cost function

The total operating cost of the MG enabling the G2V and V2G operations can be described as Eq. (65).

$$\text{OP}_{\text{cost}} = \text{OP}_{\text{cost}}^{\text{DG}} + \text{OP}_{\text{cost}}^{\text{Batt.}} + \text{OP}_{\text{cost}}^{\text{Grid}}, \ \ \forall s \in \{1, \ldots, S\} \tag{65}$$

where $\text{OP}_{\text{cost}}^{\text{DG}}$ is the operating costs of the distributed generation (CHP, PV and WT), $\text{OP}_{\text{cost}}^{\text{Batt.}}$ is the operating costs of the batteries (BESS and EV). While $\text{OP}_{\text{cost}}^{\text{Grid}}$ is the cost of buying or selling power from/to the utility grid.

The $\text{OP}_{\text{cost}}^{\text{DG}}$ is defined in Eqs. (66)–(69).

$$\text{OP}_{\text{cost}}^{\text{DG}} = \text{OP}_{\text{cost}}^{\text{CHP}} + \text{OP}_{\text{cost}}^{\text{PV}} + \text{OP}_{\text{cost}}^{\text{WT}}, \ \ \forall s \in \{1, \ldots, S\} \tag{66}$$

$$\text{OP}_{\text{cost}}^{\text{CHP}} = \sum_t^T \text{P}_{t,s}^{\text{CHP}} \times \lambda_t^{\text{CHP}}, \ \ \forall s \in \{1, \ldots, S\} \tag{67}$$

$$\text{OP}_{\text{cost}}^{\text{PV}} \sum_t^T \text{P}_{t,s}^{\text{PV}} \times \lambda_t^{\text{PV}}, \ \ \forall s \in \{1, \ldots, S\} \tag{68}$$

$$\text{OP}_{\text{cost}}^{\text{WT}} \sum_t^T \text{P}_{t,s}^{\text{WT}} \times \lambda_t^{\text{WT}}, \ \ \forall s \in \{1, \ldots, S\} \tag{69}$$

where $\text{OP}_{\text{cost}}^{\text{CHP}}$, $\text{OP}_{\text{cost}}^{\text{PV}}$ and $\text{OP}_{\text{cost}}^{\text{WT}}$ are the operating costs of the CHP, PV and WT, respectively. $\text{P}_{t,s}^{\text{CHP}}$, $\text{P}_{t,s}^{\text{PV}}$ and $\text{P}_{t,s}^{\text{WT}}$ are the power output of the CHP, PV and WT, respectively, at time t for scenario s. While λ_t^{CHP}, λ_t^{PV} and λ_t^{WT} are the utilization costs of the CHP, PV and WT, respectively.

Furthermore, $\text{OP}_{\text{cost}}^{\text{Batt.}}$ and $\text{OP}_{\text{cost}}^{\text{Grid}}$ are defined in Eqs. (70)–(73).

$$\text{OP}_{\text{cost}}^{\text{Batt.}} = \text{OP}_{\text{cost}}^{\text{BESS}} + \text{OP}_{\text{cost}}^{\text{EV}}, \ \ \forall s \in \{1, \ldots, S\} \tag{70}$$

$$\text{OP}_{\text{cost}}^{\text{BESS}} = \sum_t^T (P_{t,s}^{\text{BESS-}} \times S_t^{\text{BESS}}) - (P_{t,s}^{\text{BESS+}} \times B_t^{\text{grid}}), \ \ \forall s \in \{1, \ldots, S\} \tag{71}$$

$$\text{OP}_{\text{cost}}^{\text{EV}} = \sum_t^T (P_{t,s}^{\text{EV-}} \times S_t^{\text{EV}}) - (P_{t,s}^{\text{EV+}} \times B_t^{\text{grid}}), \ \ \forall s \in \{1, \ldots, S\} \tag{72}$$

$$\text{OP}_{\text{cost}}^{\text{Grid}} = \sum_t^T (P_{t,s}^{\text{grid-}} \times B_t^{\text{grid}}) - (P_{t,s}^{\text{grid+}} \times S_t^{\text{grid}}), \ \ \forall s \in \{1, \ldots, S\} \tag{73}$$

where $\text{OP}_{\text{cost}}^{\text{BESS}}$ and $\text{OP}_{\text{cost}}^{\text{EV}}$ are the operating costs of the BESS and EV. $P_{t,s}^{\text{BESS-}}$, $P_{t,s}^{\text{EV-}}$ and $P_{t,s}^{\text{grid-}}$ are the power supplied by BESS, EV and grid at time t for scenario s. $P_{t,s}^{\text{BESS+}}$ and $P_{t,s}^{\text{EV+}}$ are the power for charging the BESS and EV at time t for scenario s. $P_{t,s}^{\text{grid+}}$ is the excess power sold to the utility grid at time t for scenario s. While S_t^{BESS}, S_t^{EV} and S_t^{grid} are the costs of selling power from the BESS, EV and grid, respectively. B_t^{grid} is the cost of buying power from the grid to either charge the BESS, EV or supply the MG power demand.

3.2. Emission function

The proposed emission function consists of the GHG emissions from the PV, WT, CHP unit, and the emissions arising out of the power purchased from the utility grid. Hence, the emission function is expressed as in Eqs. (74)–(78).

$$\text{CD}_{\text{EM}} = \text{EM}_{\text{PV}} + \text{EM}_{\text{WT}} + \text{EM}_{\text{CHP}} + \text{EM}_{\text{Grid}} \ \ \forall s \in \{1, \ldots, S\} \tag{74}$$

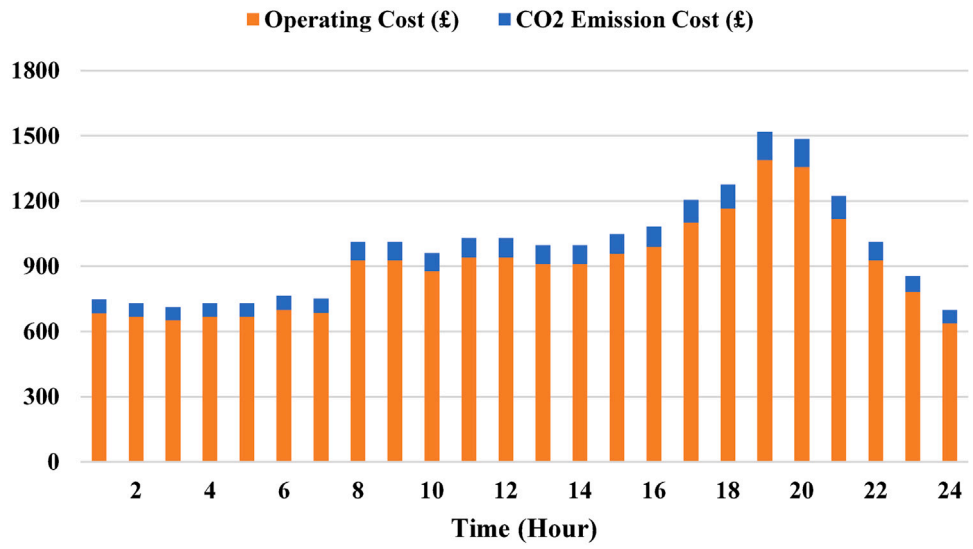

(a) Islanded mode

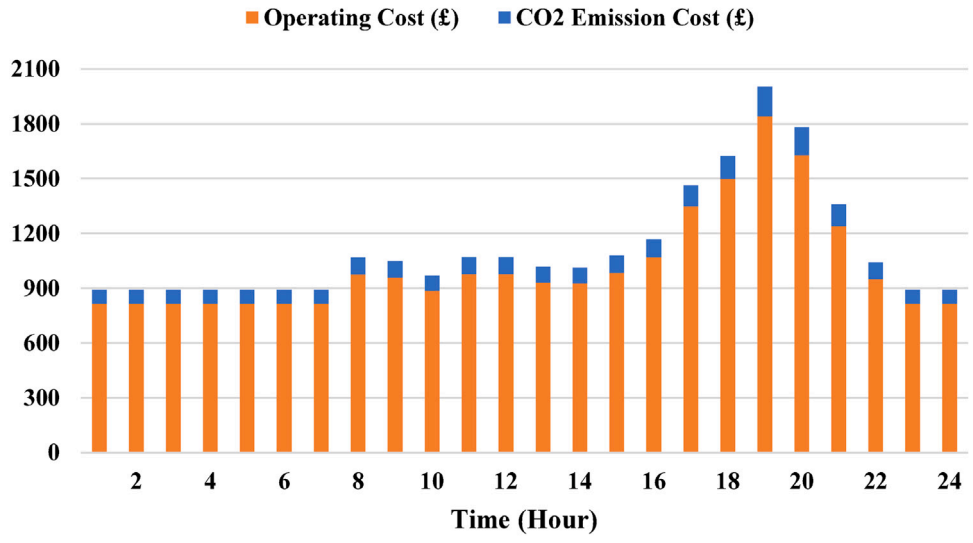

(b) Grid-connected mode

Fig. 11. Operating and CO_2 Emission Costs in **CS1** for (a) Islanded mode (b) Grid-connected modes.

$$EM_{PV} = \sum_{t}^{T} P_{t,s}^{PV} \times \gamma_t^{PV}, \quad \forall t \in \{1,\dots,T\} \text{ and } \forall s \in \{1,\dots,S\} \tag{75}$$

$$EM_{WT} = \sum_{t}^{T} P_{t,s}^{WT} \times \gamma_t^{WT}, \quad \forall t \in \{1,\dots,T\} \text{ and } \forall s \in \{1,\dots,S\} \tag{76}$$

$$EM_{CHP} = \sum_{t}^{T} P_{t,s}^{CHP} \times \gamma_t^{CHP}, \quad \forall t \in \{1,\dots,T\} \text{ and } \forall s \in \{1,\dots,S\} \tag{77}$$

$$EM_{Grid} = \sum_{t}^{T} P_{t,s}^{grid\text{-}} \times \gamma_t^{grid}, \quad \forall t \in \{1,\dots,T\} \text{ and } \forall s \in \{1,\dots,S\} \tag{78}$$

where EM_{PV}, EM_{WT}, EM_{CHP}, and EM_{Grid} are CO_2 emissions from the PV, WT, CHP unit, and utility grid, respectively. γ_t^{PV}, γ_t^{WT}, γ_t^{CHP}, and γ_t^{grid} are CO_2 emission rate of the PV, WT, CHP unit, and grid, respectively.

3.3. Grid distribution line constraint

There is a limit on the maximum apparent power that can flow through the distribution lines due to their rated voltage and cross-sectional areas as Eq. (79).

$$|P_{t,s}^{flow}| \le |\overline{P}^{flow}|, \quad \forall t \in \{1,\dots,T\} \text{ and } \forall s \in \{1,\dots,S\} \tag{79}$$

where $P_{t,s}^{flow}$ is the apparent power flowing through the distribution lines at time t for scenario s, $\overline{P}^{flow}$ is the maximum power that can flow through the lines.

3.4. Voltage limit

At any bus of the MG distribution network, the following voltage limit should be observed as Eq. (80).

$$\underline{V}^i \le V_{t,s}^i \le \overline{V}^i, \quad t = \{1,2,\dots,T\} \text{ and } \forall s \in \{1,\dots,S\} \tag{80}$$

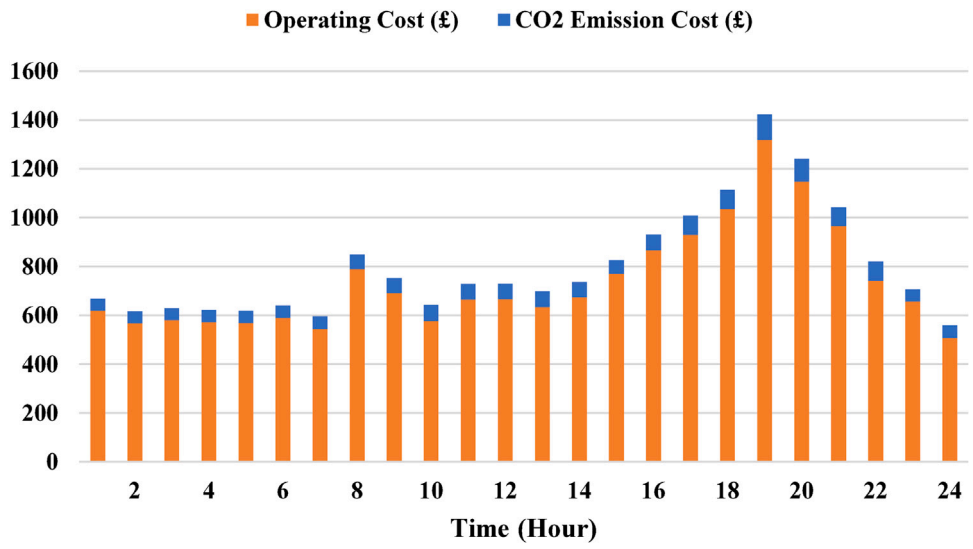

Fig. 12. Operating and CO_2 emission costs in **CS2**.

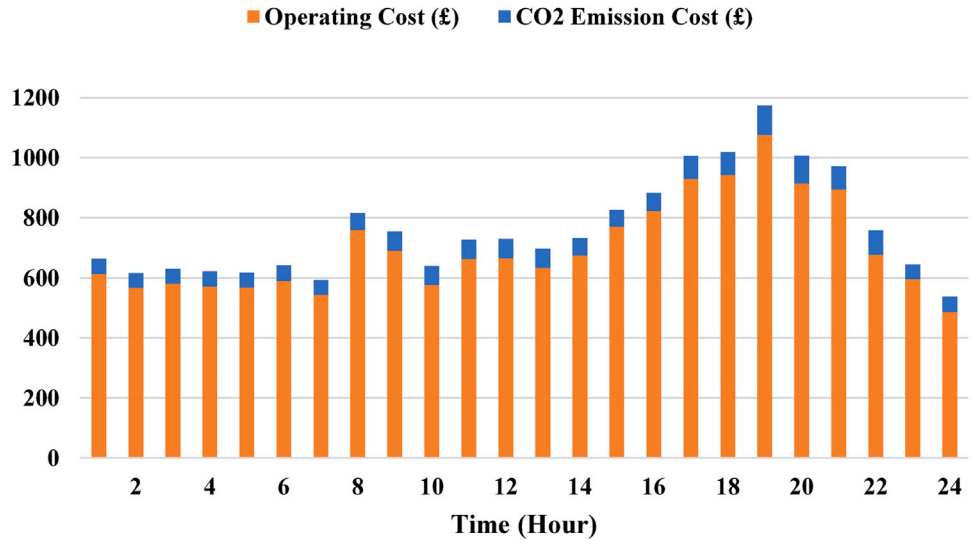

Fig. 13. Operating and CO_2 emission costs in **CS3**.

where $\underline{V}^i$ and $\overline{V}^i$ are the minimum and maximum voltage boundary, respective. $V^i_{t,s}$ is the voltage of bus i at time t for scenario s.

3.5. Battery charging and discharging constraint

The EVs' batteries and power-packs of the BESS work within permitted charging and discharging limits that must be upheld as shown in Eqs. (81)–(82).

$$P^{i+}_{t,s} \le P^{i+}_{\text{limit}} \times C^i_{t,s}, \quad i = \text{EV or BESS}$$
$$\forall t \in \{1,\dots,T\}, \quad \forall s \in \{1,\dots,S\}, \quad C \in \{0,1\} \tag{81}$$

$$P^{i-}_{t,s} \le P^{i-}_{\text{limit}} \times D^i_{t,s}, \quad i = \text{EV or BESS} \quad \forall t \in \{1,\dots,T\}, \quad \forall s \in \{1,\dots,S\},$$
$$D \in \{0,1\} \tag{82}$$

where P^{i+}_{limit} and P^{i-}_{limit} are the charging and discharging limits of the batteries, respectively. C and D are the binary variables for specifying the charging and discharging of the batteries at any given time, t. C and D are within the boundary of 0 and 1. Furthermore, the respective batteries of the EV and BESS cannot be charged and discharged concurrently. This constraint is expressed as Eq. (83).

$$C^i_{t,s} + D^i_{t,s} \le 1, \quad i = \text{EV or BESS}$$
$$\forall t \in \{1,\dots,T\}, \quad \forall s \in \{1,\dots,S\}, \quad C, D \in \{0,1\} \tag{83}$$

3.6. Power balance

The total power supplied by the connected electricity grid and distributed power generating sources must equal the total power demand at each time t for each scenario s as demonstrated in Eq. (84).

$$P^{\text{CHP}}_{t,s} + P^{\text{PV}}_{t,s} + P^{\text{WT}}_{t,s} + P^{\text{BESS-}}_{t,s} + P^{\text{grid-}}_{t,s} + P^{\text{EV-}}_{t,s} = P^{\text{EV+}}_{t,s} + P^{\text{Load}}_{t,s} + P^{\text{grid+}}_{t,s},$$
$$\forall t \in \{1,\dots,T\},$$
$$\forall s \in \{1,\dots,S\} \tag{84}$$

4. Test system

Fig. 5 illustrates the test system design. The system consists of CHP, PV, WT, and BESS integrated with the power distribution network to provide the energy required to charge the EVs and supply other loads in the system. In addition, the V2G strategy is operated to support the grid during the peak demand periods.

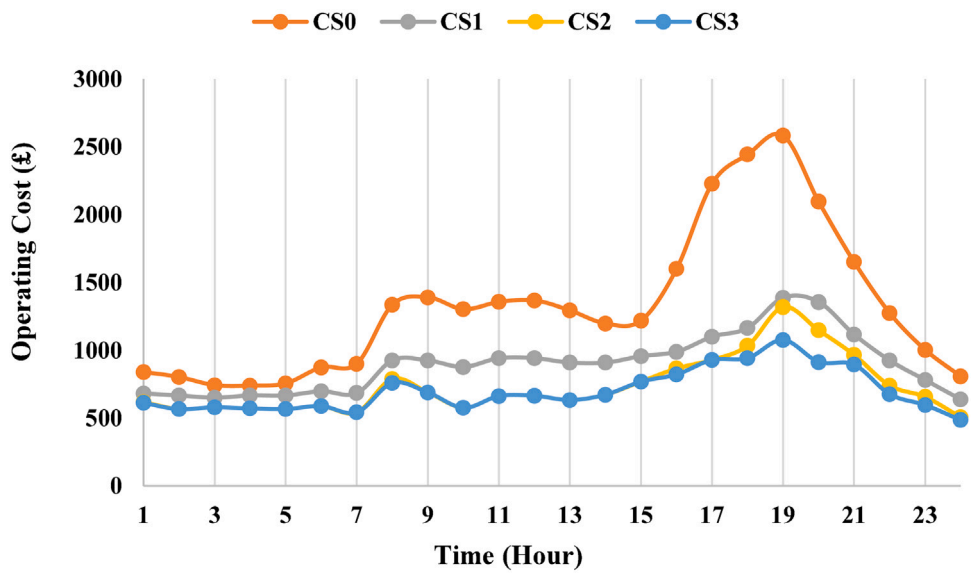

(a) Operating costs

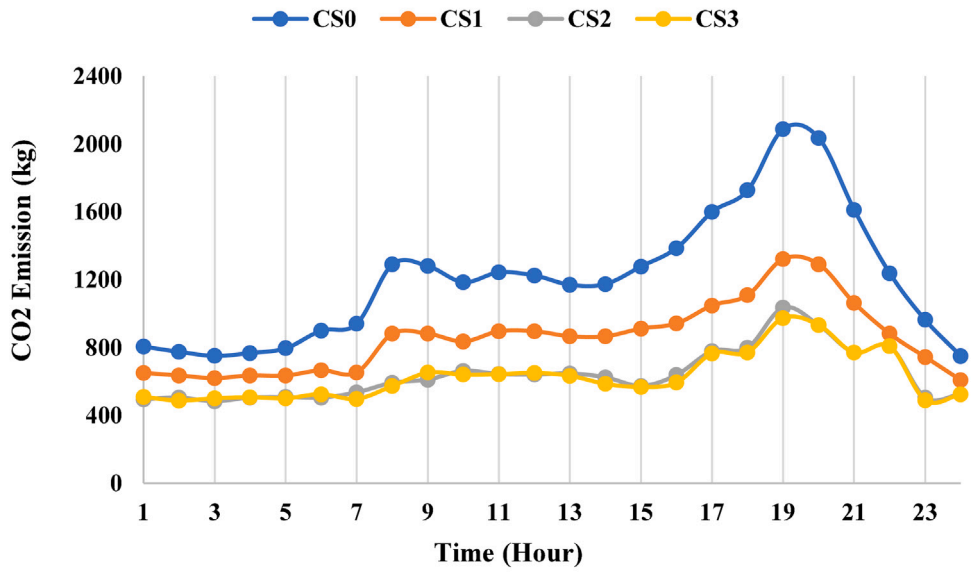

(b) CO_2 emissions

Fig. 14. Comparing (a) Operating costs (b) CO_2 emissions of the **CS0**, **CS1**, **CS2** and **CS3**.

4.1. Load forecast

Fig. 6 presents the hourly average load forecast employed in the test system. Along with the EV loads, the power generated from the CHP, PV and WT supplies MG power demand through the connected power distribution network.

4.2. CHP specifications

The CHP technologies are designed to provide about 50% to 70% of the system's hourly power load demand. The by-product heat could be utilized in buildings or other industrial processes. It should be noted that the heating demand is not taken into account in this paper and the heat generated by CHP units considered as a by-product energy. Furthermore, the amount of CHP CO_2 emission during manufacturing process and operation process is assumed to be 1.5 kg CO_2eq/MWh and 235 kg CO_2eq/MWh [43]. Table 2 highlights the input values applied in the CHP unit.

4.3. WT specifications and wind resource

A 2 MW wind turbine with a doubly fed induction generator is chosen for the test system. In addition, North East of England is selected as the installation location and has average wind speed data presented in Fig. 7 [44]. Furthermore, the carbon footprint in the life cycle of wind turbines is taken into consideration and the amount of WT CO_2 emission during manufacturing process and operation process is assumed to be 11 kg CO_2eq/MWh and 1 kg CO_2eq/MWh [45]. Table 3 highlights the key specifications of the selected wind turbine.

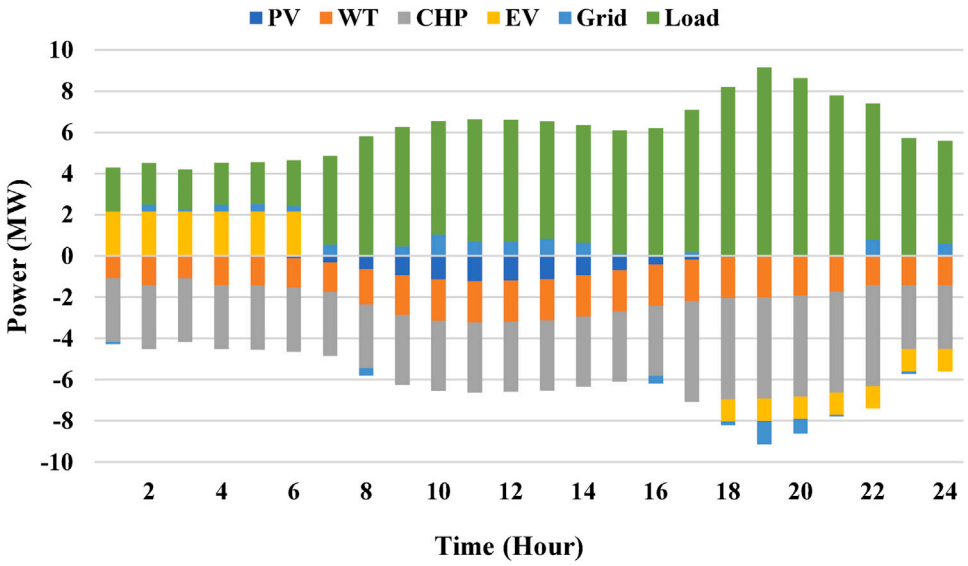

Fig. 15. The power balance of the MG network.

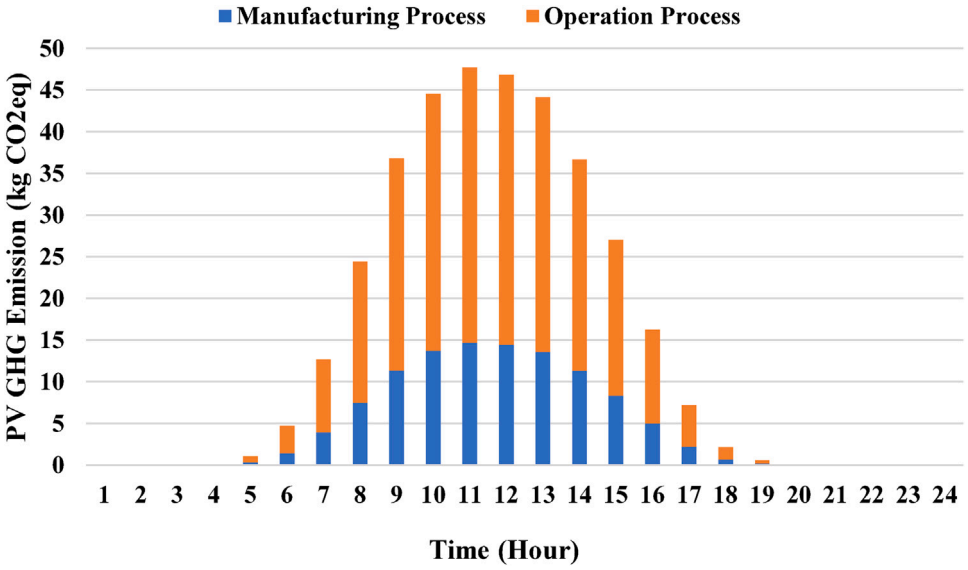

Fig. 16. LCA result for PV GHG emission.

Table 2
Input values for CHP units.

Variables	Symbol	Values
Gas turbine (GT) rating	–	4 MW
Fuel cell unit (FCU) rating	–	2 MW
Efficiency of GT	η_{PGU}	48.3%
Efficiency of FCU	η_{FCU}	60%
Efficiency of fuel reformer	η_{FR}	74%
Efficiency of heat recovery unit	η_{HRU}	80%
Efficiency of heating coil	η_{HC}	80%
Efficiency of boiler	η_{BOILER}	94%
Price of natural gas	$cost_{NG}$	£4.88/MMBtu
Natural gas emission rate	Em_{NG}	150 kg CO_2/MWh

4.4. PV specifications and solar resource

A 380 W PV panel is used in the test system. The PV panel is designed to optimize energy generation and has a product and power coverage warranty of 40 years. In addition, the carbon footprint of PV during manufacturing process and operation process is assumed to be 12 kg CO_2eq/MWh and 27 kg CO_2eq/MWh [47]. Table 4 shows the PV's key specifications, and Fig. 8 presents the hourly solar irradiance of the selected installation site, North East England [48].

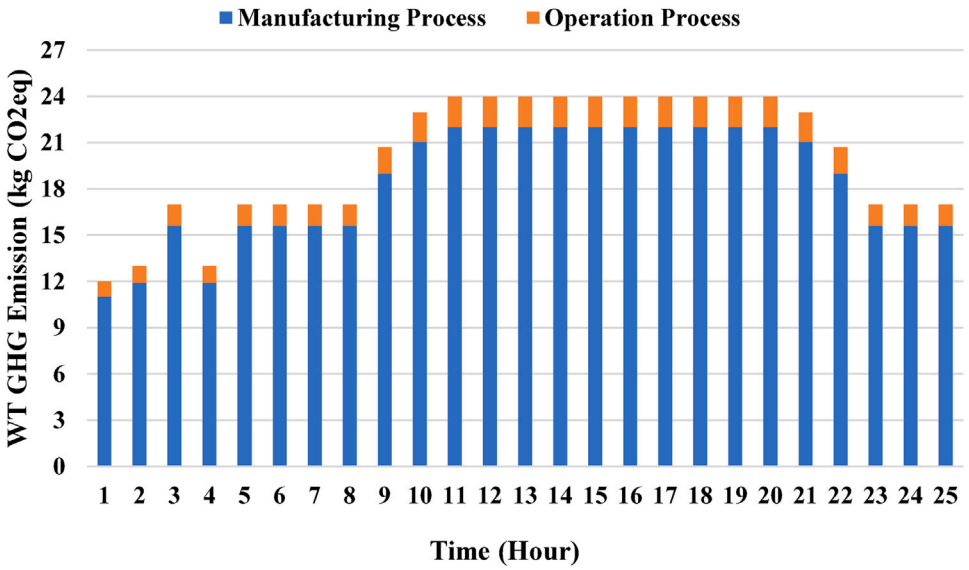

Fig. 17. LCA result for WT GHG emission.

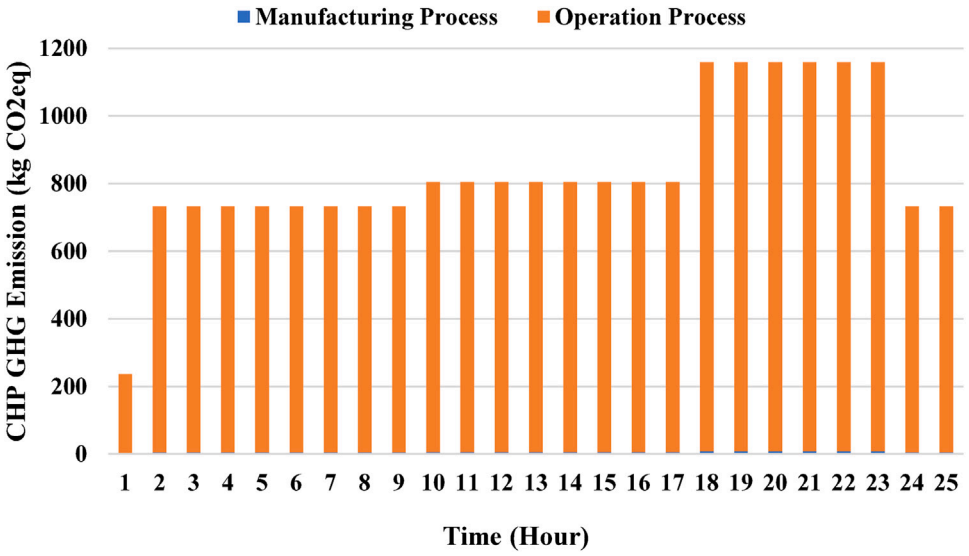

Fig. 18. LCA result for CHP GHG emission.

Table 3
Wind turbine specifications [46].

Specifications	Values
Rated generator output	2000 kW
Diameter	80 m
Swept area	4978 m^2
Blade length	39 m
Cut-in wind speed	4 m/s
Cut-out wind speed	25 m/s

4.5. EV and BESS specifications

Only a few EVs are currently built to support V2G operations. Hence, the Kia Soul EV is selected for the test system. Conversely, the Tesla power-pack is used for the BESS. The BESS is installed to support V2G operation during peak demand, reduce the intermittent nature of the added RESs and minimize energy wastage by storing the excess energy from the CHP and electricity grid. Also, the BESS is configured to a minimum and maximum state of charge (SoC) of 10% and 95%, respectively. Table 5 and Table 6 highlight the chosen EV and power-pack specifications, respectively.

4.6. Grid supply and electricity prices

The test system design is integrated with the power distribution network for easy and low-cost evacuation of the power generated from the CHP, PV, and WT. Also, the distribution network acts as a medium for the sales or purchase of excess or shortage power, respectively. Therefore, the average hourly price of grid electricity for North East England is deployed in the test system. Fig. 9 shows the grid electricity prices [49] and CO_2 emissions [50].

5. Results and discussions

For the sake of a detailed analysis, four case studies (**CSs**) are defined in this paper as follows:

Table 4
PV panels specifications [51].

Specifications	Values
Material	Monocrystalline
Maximum annual degradation	25%
Nominal power	380 W
Panel efficiency	21.5%
Panel area	1.76 m^2

Table 5
EV specifications [52].

Specifications	Values
Battery	64 kWh Li-ion polymer battery
Maximum power	150 kW
AC charge time (230 V)	29 h (0% → 100%)
AC charge time (7.2 kW)	9 h 35 mins (0% → 100%)
DC charge time (50 kW)	1 h 15 mins (0% → 80%)
DC charge time (100 kW)	54 mins (0% → 80%)
Battery	64 kWh Li-ion polymer battery

Table 6
BESS specifications [52].

Specifications	Values
Depth of discharge	100%
Energy capacity	Up to 232 kWh (AC)
Power	Up to 130 kW (AC)
Scalable inverter power	70 kVA to 700 kVA (at 480 V)
System efficiency	88% round trip (2 h system) 89.5% round trip (5 h system)

5.1. CS0

In **CS0**, electricity from the existing power distribution network supplies the EVs and forecasted MG power demand. Hence, the electricity prices and CO_2 emission rates applied are for the utility grid. Fig. 10 illustrates the hourly operating cost and CO_2 emission cost in this test case and forms the reference base for other test cases in this research. There are no operational costs or CO_2 minimization under this CS, as both objective functions are driven solely by the set prices of the utility operators, hourly load demands and the types of power generating plants installed upstream. Therefore, the daily average operating and CO_2 emission costs in this CS are approximately £31,820 and £2,898, respectively.

5.2. CS1: Only CHP

This CS investigates the impacts of deploying the harmonized natural gas and hydrogen fuel cell CHP technologies in facilitating the G2V operations of the EVs in addition to the MG power demand. Firstly, the CHP is operated in an islanded mode (without grid integration) to achieve a better impact system analysis. Lastly, it is used and analysed in a grid-connected mode. Hence, Fig. 11 presents hourly operating costs and CO_2 emission costs in the islanded and grid-connected operating modes. In comparing the CHP's operations in the islanded mode with **CS0**, the daily operating costs declined to around £21,568.1, which represents a 32.22% reduction, while the CO_2 emissions plummeted to £2,053.6, a 29.13% decrease in reference to **CS0**. Similarly, 23.00% and 20.89% reductions were achieved in the operating costs and CO_2 emission costs of the grid-connected mode, respectively. The lower percentage deduction in the grid-connected mode is due to higher operating costs and CO_2 emissions from the purchased grid power. However, an estimated 659.3 MMBTU/day of heat recovered from the CHP in islanded mode is more than the 622.1 MMBTU/day of heat retrieved in the grid-connected mode, as more power is produced from the CHP to meet the electricity demand, which facilitates the recovery of more by-product heat.

5.3. CS2: With CHP, PV, WT and grid supply (no BESS)

CS2 examines the benefits of adding PV, WT, and national grid to the **CS1**. This approach further minimizes the MG's operating and CO_2 emission costs, as demonstrated in Fig. 12. In this CS, the daily operating and emission expenses derived for the MG are about £17,663.8 and £1,532.2. When compared with **CS0**, **CS2** leads to a 44.49% and 47.13% reduction in operating and CO_2 emission costs, respectively. Similarly, **CS2** sees an 18.10% and 25.39% decline when set side by side with **CS1** (islanded mode), while 27.90% and 33.16% were achieved when compared with the grid-connected method of **CS1**. Hence, the derived reduction in the two objective functions highlights the impacts of the PV and WT added to the system. Finally, about 365.10 MMBTU/day of heat is recovered from the CHP.

5.4. CS3: *CS2* and BESS (V2G and G2V operations)- without BESS degradation cost

This CS cross-examines the impacts of the V2G strategy on the MG and the advantages of the BESS in supporting V2G operations. Fig. 13 shows the test case's hourly operating and CO_2 emission costs. In this research, the V2G facility is employed for 6 h a day during the high prices of the electricity. In addition, the BESS primarily acts to support the V2G operations when the power supplied by the EV batteries is not enough to meet the MG's high demand. However, the BESS is also deployed when there is power shortage from the connected utility grid or at periods of high electricity prices. Conversely, the BESS is charged during hours of low power demand and low electricity prices. In this CS, the MG operating and CO_2 emission costs declined by 47.20% and 47.90%, respectively, compared to **CS0**. The achieved lower minimization values demonstrate the impact of the V2G and BESS integration. Furthermore, compared with **CS1** and **CS2**, the operating costs plummeted by 22.10% and 4.88%, respectively, while the CO_2 emission costs reduced by 26.48% and 1.46%, respectively. Fig. 14 compares the **CS0**, **CS1**, **CS2** and **CS3** of the MG operating costs and CO_2 emissions. It is evident that **CS3** provides the best minimization of the objective functions, having achieved total daily operating costs of around £16,801.67 and daily CO_2 emission costs of £1,509.8.

5.5. MG power balance

Fig. 15 presents the power balance for **CS3**, which considers the whole MG system consisting of the CHP, PV, WT, BESS, utility grid and V2G strategy. From the system's power balance, it is observed that the CHP, PV, WT, BESS (V2G operations), and utility grid contribute an average of 59.16%, 6.11%, 27.54%, 5.11% and 2.08%, respectively, in meeting the daily power demands for the G2V operations and forecasted MG power demand. Furthermore, around 14.18% of the daily generated power from the CHP and RES is sold to the utility grid as excess power, providing additional revenue for MG's operations.

5.6. LCA results

Figs. 16–18 represent the LCA results of the GHG emissions of the PV, WT, and CHP unit, respectively. It can be noted that 353.13 kg CO_2eq, 489.38 kg CO_2eq, and 20717.41 kg CO_2eq are emitted during a 24-hour time horizon scheduling of the PV, WT, and CHP unit, respectively. It is clear that applying RES-based units such as PVs and WTs have a significant impact on reducing global warming factor (CO_2eq) and the corresponding emission costs.

6. Conclusion

This paper proposes a stochastic operation of the power distribution networks via minimizing the operating and CO_2 emissions costs. It examines the integration multi-energy technologies considering the uncertainties of RES generation, load consumption, and charging/discharging periods using the scenario-based analysis method. This paper also successfully analyses the benefits of applying CHP technologies alongside PV and WT in facilitating the mass deployment of EVs to decarbonize the transport sector and contribute to achieving the Net-Zero goal. In addition, the research provides a complex problem formation of harmonized natural gas and hydrogen fuel cell CHP technologies following a hybrid electric-thermal load strategy. Correspondingly, it investigates the integration of BESS in storing the excess power from the CHP and RES, and supporting the V2G operations of the EVs at high power demand periods. Furthermore, the research explores the EVs' scheduled G2V and V2G strategies. The G2V process happens during base demand periods at low market prices and CO_2 emissions, while the V2G operation is planned for high demand periods when the MG's electricity prices and CO_2 emissions are high. Finally, the MG design was tested in four diverse CSs and the LCA impact was investigated to calculate the CO_2 emissions of the distributed generation units.

The main results of the simulations are achieved as follows:

1. In reference to the **CS0**, 23.00% and 20.89% decrease in the MG's operating costs and CO_2 emissions were obtained when deploying only the grid-connected CHP technologies to facilitate the EVs' G2V operations.
2. Applying the CHP, PV, and WT further reduces the MG's operating costs by 44.49% and CO_2 emissions by 47.13%.
3. Adding the BESS to support the EVs' V2G operations extends the design's impact on the MG's operating costs and CO_2 emissions, lowering them to 47.20% and 47.90%, respectively.

Therefore, the achieved results showcase the economic and environmental benefits of applying CHP technologies with RES and BESS in enabling the mass use of EVs to achieve sustainable decarbonization of the transport sector and contribute to achieving the global Net-Zero goal. According to the architecture of the proposed network, the multi-carrier energy systems can be also studied in future researches. Likewise, multi-energy storage system can be applied in the energy systems to realize a comprehensive analysis for the optimal operation of the energy resources. In addition, the self-healing concepts can also be proposed to investigate the operation potentials in the isolated mode.

CRediT authorship contribution statement

Alex S. Daramola: Conceptualization, Methodology, Software, Visualization, Investigation. **Seyed Ehsan Ahmadi:** Data curation, Conceptualization, Writing – original draft. **Mousa Marzband:** Conceptualization, Methodology, Writing, Supervision, Validation. **Augustine Ikpehai:** Supervision, Validation.

Declaration of competing interest

The authors declare that they have no known competing financial interests or personal relationships that could have appeared to influence the work reported in this paper.

Data availability

No data was used for the research described in the article.

Acknowledgements

This work was supported from DTE Network+ funded by EPSRC, United Kingdom grant reference EP/S032053/1.

References

[1] A. Hill, L. Martinez-Diaz, Building a Resilient Tomorrow: How to Prepare for the Coming Climate DisruptionHow to Prepare for the Coming Climate Disruption, Oxford University Press, New York, 2020.
[2] J. Rissman, C. Bataille, E. Masanet, N. Aden, W.R. Morrow, N. Zhou, N. Elliott, R. Dell, N. Heeren, B. Huckestein, J. Cresko, S.A. Miller, J. Roy, P. Fennell, B. Cremmins, T. Koch Blank, D. Hone, E.D. Williams, S. de la Rue du Can, B. Sisson, M. Williams, J. Katzenberger, D. Burtraw, G. Sethi, H. Ping, D. Danielson, H. Lu, T. Lorber, J. Dinkel, J. Helseth, Technologies and policies to decarbonize global industry: Review and assessment of mitigation drivers through 2070, Appl. Energy 266 (2020).
[3] R. Reitz, H. Ogawa, R. Payri, T. Fansler, S. Kokjohn, Y. Moriyoshi, A. Agarwal, D. Arcoumanis, D. Assanis, C. Bae, K. Boulouchos, M. Canakci, S. Curran, I. Denbratt, M. Gavaises, M. Guenthner, C. Hasse, Z. Huang, T. Ishiyama, B. Johansson, T. Johnson, G. Kalghatgi, M. Koike, S. Kong, A. Leipertz, P. Miles, R. Novella, A. Onorati, M. Richter, S. Shuai, D. Siebers, W. Su, M. Trujillo, N. Uchida, B. Vaglieco, R. Wagner, H. Zhao, IJER editorial: The future of the internal combustion engine, Int. J. Engine Res. 21 (1) (2020) 3–10.
[4] L. Rivera-González, D. Bolonio, L.F. Mazadiego, S. Naranjo-Silva, K. Escobar-Segovia, Long-term forecast of energy and fuels demand towards a sustainable road transport sector in Ecuador (2016–2035): A LEAP model application, Sustainability (Switzerland) 12 (2) (2020).
[5] R. Salem, A. Bahadori-Jahromi, A. Mylona, P. Godfrey, D. Cook, Comparison and evaluation of the potential energy, carbon emissions, and financial impacts from the incorporation of CHP and CCHP systems in existing UK hotel buildings, Energies 11 (5) (2018).
[6] M. Alinejad, O. Rezaei, A. Kazemi, S. Bagheri, An optimal management for charging and discharging of electric vehicles in an intelligent parking lot considering vehicle owner's random behaviors, J. Energy Storage 35 (2021).
[7] G. Merhy, A. Nait-Sidi-Moh, N. Moubayed, Control, regulation and optimization of bidirectional energy flows for electric vehicles' charging and discharging, Sustainable Cities Soc. 57 (2020).
[8] D. Sadeghi, S.E. Ahmadi, N. Amiri, Satinder, M. Marzband, A. Abusorrah, M. Rawa, Designing, optimizing and comparing distributed generation technologies as a substitute system for reducing life cycle costs, CO2 emissions, and power losses in residential buildings, Energy 253 (2022) 123947.
[9] S.E. Ahmadi, D. Sadeghi, M. Marzband, A. Abusorrah, K. Sedraoui, Decentralized bi-level stochastic optimization approach for multi-agent multi-energy networked micro-grids with multi-energy storage technologies, Energy 245 (2022) 123223.
[10] P. Mancarella, MES (multi-energy systems): An overview of concepts and evaluation models, Energy 65 (2014) 1–17.
[11] P. Mancarella, G. Andersson, J. Peças-Lopes, K. Bell, Modelling of integrated multi-energy systems: Drivers, requirements, and opportunities, in: 2016 Power Systems Computation Conference, PSCC, 2016, pp. 1–22.
[12] J. Zhao, H. Chang, X. Luo, Z. Tu, S.H. Chan, Dynamic analysis of a CCHP system based on fuel cells integrated with methanol-reforming and dehumidification for data centers, Appl. Energy 309 (2022) 118496.
[13] L. Fan, Z. Tu, X. Luo, S.H. Chan, MW cogenerated proton exchange membrane fuel cell combined heat and power system design for eco-neighborhoods in north China, Int. J. Hydrogen Energy 47 (6) (2022) 4033–4046.
[14] J. Zhao, S. Cai, X. Huang, X. Luo, Z. Tu, 4E analysis and multiobjective optimization of a PEMFC-based CCHP system with dehumidification, Energy Convers. Manage. 248 (2021) 114789.
[15] S. Cai, X. Li, S. Li, X. Luo, Z. Tu, Flexible load regulation method for a residential energy supply system based on proton exchange membrane fuel cell, Energy Convers. Manage. 258 (2022) 115527.
[16] M. Taljegard, L. Göransson, M. Odenberger, F. Johnsson, Impacts of electric vehicles on the electricity generation portfolio – a Scandinavian-German case study, Appl. Energy 235 (2019) 1637–1650.
[17] R. Zhang, S. Fujimori, The role of transport electrification in global climate change mitigation scenarios, Environ. Res. Lett. 15 (3) (2020).
[18] C.B. Robledo, V. Oldenbroek, F. Abbruzzese, A.J. van Wijk, Integrating a hydrogen fuel cell electric vehicle with vehicle-to-grid technology, photovoltaic power and a residential building, Appl. Energy 215 (2018) 615–629.
[19] Z. Liu, Q. Wu, S. Huang, L. Wang, M. Shahidehpour, Y. Xue, Optimal day-ahead charging scheduling of electric vehicles through an aggregative game model, IEEE Trans. Smart Grid 9 (5) (2018) 5173–5184.
[20] B. Sun, Z. Huang, X. Tan, D.H.K. Tsang, Optimal scheduling for electric vehicle charging with discrete charging levels in distribution grid, IEEE Trans. Smart Grid 9 (2) (2018) 624–634.
[21] Y. Zhang, P. You, L. Cai, Optimal charging scheduling by pricing for EV charging station with dual charging modes, IEEE Trans. Intell. Transp. Syst. 20 (9) (2019) 3386–3396.
[22] R. Das, Y. Wang, G. Putrus, R. Kotter, M. Marzband, B. Herteleer, J. Warmerdam, Multi-objective techno-economic-environmental optimisation of electric vehicle for energy services, Appl. Energy 257 (2020) 113965.
[23] A. Modarresi Ghazvini, J. Olamaei, Optimal sizing of autonomous hybrid PV system with considerations for V2G parking lot as controllable load based on a heuristic optimization algorithm, Sol. Energy 184 (2019) 30–39.

[24] M.J. Morshed, J.B. Hmida, A. Fekih, A probabilistic multi-objective approach for power flow optimization in hybrid wind-PV-PEV systems, Appl. Energy 211 (2018) 1136–1149.
[25] J. Zhong, X. Xiong, An orderly EV charging scheduling method based on deep learning in cloud-edge collaborative environment, Artif. Intell. Internet Things (IoT) Civ. Eng. 184 (2021) 30–39.
[26] M. Shamshirband, J. Salehi, F.S. Gazijahani, Decentralized trading of plug-in electric vehicle aggregation agents for optimal energy management of smart renewable penetrated microgrids with the aim of CO_2 emission reduction, J. Clean. Prod. 200 (2018) 622–640.
[27] D. Li, S. Guo, W. He, M. King, J. Wang, Combined capacity and operation optimisation of lithium-ion battery energy storage working with a combined heat and power system, Renew. Sustain. Energy Rev. 140 (2021) 110731.
[28] ISO 14040:2006 Environmental management — Life cycle assessment — Principles and framework, https://www.iso.org/standard/37456.html.
[29] R. Turconi, Life cycle assessment of electricity systems, 2014.
[30] J. Sadhukhan, S. Sen, S. Gadkari, The mathematics of life cycle sustainability assessment, J. Clean. Prod. 309 (2021) 127457.
[31] S.E. Ahmadi, N. Rezaei, An IGDT-based robust optimization model for optimal operational planning of cooperative microgrid clusters: A normal boundary intersection multi-objective approach, Int. J. Electr. Power Energy Syst. 127 (2021) 106634.
[32] H. Heitsch, W. Römisch, Scenario reduction algorithms in stochastic programming, Scenario Reduct. Algorithms Stoch. Program. 24 (2) (2003) 187–206.
[33] S.E. Ahmadi, N. Rezaei, A new isolated renewable based multi microgrid optimal energy management system considering uncertainty and demand response, Int. J. Electr. Power Energy Syst. 118 (2020) 105760.
[34] P.J. Mago, L.M. Chamra, Analysis and optimization of CCHP systems based on energy, economical, and environmental considerations, Renew. Sustain. Energy Rev. 40 (2009) 1099–1106.
[35] P. Mago, L. Chamra, J. Ramsay, Micro-combined cooling, heating and power systems hybrid electric-thermal load following operation, Appl. Therm. Eng. 30 (8) (2010) 800–806.
[36] S.E. Ahmadi, M. Marzband, A. Ikpehai, A. Abusorrah, Optimal stochastic scheduling of plug-in electric vehicles as mobile energy storage systems for resilience enhancement of multi-agent multi-energy networked microgrids, J. Energy Storage 55 (2022) 105566.
[37] P. Fazlalipour, M. Ehsan, B. Mohammadi-Ivatloo, Risk-aware stochastic bidding strategy of renewable micro-grids in day-ahead and real-time markets, Energy 171 (2019) 689–700.
[38] A novel falling model for wind speed probability distribution of wind farms, Renew. Energy 184 (2022) 91–99.
[39] J. Wang, B. Yang, D. Li, C. Zeng, Y. Chen, Z. Guo, X. Zhang, T. Tan, H. Shu, T. Yu, Photovoltaic cell parameter estimation based on improved equilibrium optimizer algorithm, Energy Convers. Manage. 236 (2021) 114051.
[40] C. Xie, D. Wang, C.S. Lai, R. Wu, X. Wu, L.L. Lai, Optimal sizing of battery energy storage system in smart microgrid considering virtual energy storage system and high photovoltaic penetration, J. Clean. Prod. 281 (2021) 125308.
[41] S.E. Ahmadi, N. Rezaei, H. Khayyam, Energy management system of networked microgrids through optimal reliability-oriented day-ahead self-healing scheduling, Sustain Energy Grids Netw 23 (2020) 100387.
[42] X. Wen, D. Abbes, B. Francois, Stochastic optimization for security-constrained day-ahead operational planning under PV production uncertainties: Reduction analysis of operating economic costs and carbon emissions, IEEE Access 9 (2021) 97039–97052.
[43] F. Meng, G. Dillingham, Life cycle analysis of natural gas-fired distributed combined heat and power versus centralized power plant, Energy Fuels 32 (11) (2018) 11731–11741.
[44] visualcrossing, Weather Query Builder, https://www.visualcrossing.com/weather/weather-data-services.
[45] S. Peach, Carbon footprint of a wind turbine, 2021, https://shorturl.at/cBEV7.
[46] Hitachi, Wind Turbine, https://www.hitachi.com/products/energy/wind/products/htw2000_80/specification/index.html.
[47] Cool Effect, Carbon Footprint of Solar Panel Manufacturing, https://www.cooleffect.org/solar-carbon-footprint.
[48] European Commission, Photovoltaic Geographical Information System, https://re.jrc.ec.europa.eu/pvg_tools/en/tools.html#PVP.
[49] energy-stats.uk, User configurable dashboard, https://shorturl.at/iACX5.
[50] Nationalgrid ESO, Historical Generation Mix and Carbon Intensity, https://data.nationalgrideso.com/data-groups/carbon-intensity1.
[51] SunPower, SunPower Maxeon Solar Panels, https://sunpower.maxeon.com/uk/sites/default/files/2022-03/sp_max3_104c_com_380-400_dc_ds_en_a4_544454.pdf.
[52] Kia U.K. Limited, The Soul EV, https://www.kia.com/content/dam/kwcms/kme/uk/en/assets/vehicles/soul-ev/specification/kia-soul-ev-specification.pdf.